Investigation of spectroscopic, reactive, transport and docking properties of 1-(3,4-dichloropheny1)-3[3-(trifluoromethyl)phenyl] thiourea (ANF-6): Combined experimental and computational study

Accepted Manuscript

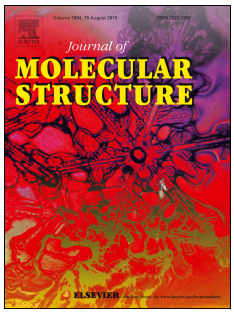

Investigation of spectroscopic, reactive, transport and docking properties of 1-(3,4-dichlorophenyl)-3-[3-(trifluoromethyl)phenyl]thiourea (ANF-6): Combined experimental and computational study

V.V. Aswathy, Y. Sheena Mary, P.J. Jojo, C. Yohannan Panicker, Anna Bielenica, Stevan Armaković, Sanja J. Armaković, Paulina Brzózka, Sylwester Krukowski, C. Van Alsenoy

PII: S0022-2860(17)30016-9

DOI: 10.1016/j.molstruc.2017.01.016

Reference: MOLSTR 23321

To appear in: *Journal of Molecular Structure*

Received Date: 31 July 2016

Revised Date: 28 December 2016

Accepted Date: 4 January 2017

Please cite this article as: V.V. Aswathy, Y.S. Mary, P.J. Jojo, C.Y. Panicker, A. Bielenica, S. Armaković, S.J. Armaković, P. Brzózka, S. Krukowski, C. Van Alsenoy, Investigation of spectroscopic, reactive, transport and docking properties of 1-(3,4-dichlorophenyl)-3-[3-(trifluoromethyl)phenyl]thiourea (ANF-6): Combined experimental and computational study, *Journal of Molecular Structure* (2017), doi: 10.1016/j.molstruc.2017.01.016.

Graphical abstract: Investigation of spectroscopic, reactive, transport and docking properties of 1-(3,4-dichlorophenyl)-3-[3-(trifluoromethyl)phenyl]thiourea (ANF-6): combined experimental and computational study

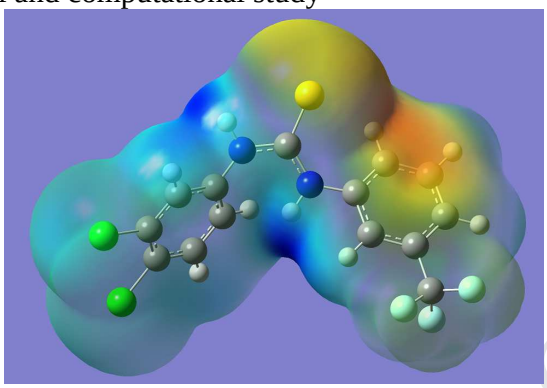

Investigation of spectroscopic, reactive, transport and docking properties of 1-(3,4-dichlorophenyl)-3-[3-(trifluoromethyl)phenyl]thiourea (ANF-6): combined experimental and computational study

Aswathy V.V[a], Sheena Mary Y[b]*, P.J.Jojo[b], C.Yohannan Panicker[a], Anna Bielenica[c], Stevan Armaković[d], Sanja J. Armaković[e], Paulina Brzózka[f], Sylwester Krukowski[f], C.Van Alsenoy[g]

[a]Department of Physics, TKM College of Arts and Science, Kollam, Kerala, India.

[b]Department of Physics, Fatima Mata National College, Kollam, Kerala, India.

[c] Chair and Department of Biochemistry, Medical University of Warsaw, 02-097, Warszawa, Poland.

[d]University of Novi Sad, Faculty of Sciences, Department of Physics, Trg D. Obradovića 4, 21000 Novi Sad, Serbia

[e]University of Novi Sad, Faculty of Sciences, Department of Chemistry, Biochemistry and Environmental Protection, Trg D. Obradovića 3, 21000 Novi Sad, Serbia

[f]Department of Inorganic and Analytical Chemistry, Faculty of Pharmacy, Medical University of Warsaw, 02-097 Warszawa, Poland..

[g]Department of Chemistry, University of Antwerp, Groenenborgerlaan 171, B-2020, Antwerp, Belgium

*Author for correspondence: email:sypanicker@rediffmail.com

Abstract

The wavenumbers, molecular structure, molecular electrostatic potential, nonlinear optical properties and natural bond orbital analysis of a thiourea derivative, 1-(3,4-dichlorophenyl)-3-[3-(trifluoromethyl)phenyl]thiourea (ANF-6) were reported. For the title molecule, HOMO is all over the molecule except the CF_3 group and LUMO is over the 1,3-substituted phenyl ring PhII, CF_3 group and C-S group. The most reactive sites of the molecule are identified with the help of MEP plot analysis. The first hyperpolarizability of the title compound is 38.69 times that of the standard NLO material urea. This study also encompassed the investigation of local reactivity properties by calculation of average local ionization energies and Fukui functions, which values have been mapped to the electron density surface. Bond dissociation energies have been calculated for all single acyclic bonds in order to assess the possibilities for autoxidation process and to determine where degradation could start. Radial distribution functions after molecular dynamics simulations have been calculated in order to determine the atoms with the most pronounced interactions with water. Within Marcus semi-

empiric approach, charge hopping properties of the title molecule have been assessed and compared with urea and thiourea molecules. From the molecular docking study, the docked title compound forms a stable complex with cytochrome reductase and got a binding affinity value of -6.3 kcal/mol and hence the title compound can be a lead compound for developing new antifungal agent.

Keywords: DFT; Thiourea; ALIE; BDE; RDF; Docking.

1. Introduction:

Over the last several years, the important role of thiourea derivatives in the field of new chemotherapeutics development is undisputed, due to their significant antibacterial [1-3], antifungal [4,5], anti-tubercular [2, 6] and cytotoxic [1, 2, 7-9] properties. Their significant inhibitory effect on the growth of *Staphylococcus epidermidis* and *Staphylococcus aureus* strains is the result of a blockade of bacterial topoisomerase IV and/or gyrase action [1, 2, 10]. What is more, these thiourea-based derivatives possessing a halogen atom in their structure are known to inhibit and disperse bacterial bio-film [1, 2, 11]. According also to other author findings, fluorine-containing arylthiourea molecules express higher biological activity when compared to analogs with electron-donating substituent [1, 2, 12, 13]. Simultaneously, di-substituted derivatives are more active than mono-substituted halogen connections, as they exert stronger electronegative effect [1, 2, 5, 14, 15]. The title compound 3-(trifluoromethyl)phenyl-thiourea was found as a powerful inhibitor of the growth of standard and hospital methicillin-resistant staphylococcal strains; it also turned out as cytotoxic against MT-4 cells and reduced a proliferation of human leukaemia/lymphoma cell lines [1]. Popularity of compounds based on thiourea has been demonstrated by numerous other studies. From the aspect of organocatalysis it is important to mention the work by Koutoulogenis et al. [16]. Just recently they have reported synthesis of functionalized six-membered rings with multiple chiral centers mediated by thiourea. Coordination, biological and structural properties of thiourea derivatives have been thoroughly processed in the article reported by Saeed et al. [17]. Simplicity of synthesis of various thiourea derivatives and their possibility to form two hydrogen bonds with anion are another property emphasizing the great potential of thiourea based compounds [18]. Thiourea compounds also have significant potential in the material science. For example these compounds can form multiple inter- and intra-molecular hydrogen bonds thanks to which some amidothiourea compounds have been efficiently utilized as colorimetric and fluorescent anions sensors [19]. Thiourea compounds also have the possibility to be applied as OLED materials as well, thanks to the lone pairs of nitrogen, sulfur and oxygen atoms [20]. The aim of this work was to thoroughly investigate title

molecule by spectroscopic characterization and by computational investigation or reactive properties. IR, Raman and NMR spectroscopic approaches have been employed for characterization, while computational prediction of reactive properties has been performed by density functional theory (DFT) calculations and molecular dynamics (MD) simulations. To validate the used level of theory experimentally and theoretically obtained spectra haven compared. Computational study of reactivity encompassed both global and local reactive properties. Global reactivity properties have been assessed by frontier molecular orbitals thanks to which quantum-molecular descriptors such as HOMO-LUMO gap, global hardness and electrophilicity have been calculated. Local reactivity properties have been assessed by inspection of charge distribution according to molecular electrostatic potential (MEP) surfaces, average local ionization energy (ALIE) surfaces and Fukui functions. In this work we have also investigated sensitivity of title molecule towards autoxidation and hydrolysis mechanisms. Both of these mechanisms are important from the ecological aspect, concretely for the understanding of degradation properties of title molecule. Pharmaceutical molecules such as thiourea derivatives have been detected in all types of water and therefore they are great threat for aquatic organisms [21-23]. Degradation of such molecules is very under natural conditions and standard water purification methods are not suitable. However, in these cases forced degradation based on advanced oxidation processes has been seen as efficient alternative [24-26]. Bond dissociation energy (BDE) for hydrogen abstraction is closely related to the autoxidation properties and can be used for the determination of important reactive molecule sites. Since great majority of pharmaceutical molecules eventually end up in some kind of water, it is also useful to investigate how water influences such molecules. In this regard it is useful to calculate radial distribution functions which can effectively indicate which atoms have pronounced interactions with water molecules and therefore indicate the effects of hydrolysis. Due to the fact that thiourea compounds have significant potential for the application in the area of organic electronics, we have also decided to investigate transport properties of the title molecule. Namely, applying the concept of Marcus semi empiric approach we have calculated charge transfer rates of holes and electrons.

2. Experimental details

The preparation of 1-(3,4-dichlorophenyl)-3-[3-(trifluoromethyl)phenyl]thiourea

A solution of starting 3-(trifluoromethyl)aniline (0.0031 mol, 0.50 g) in anhydrous acetonitrile (10 mL) was treated with 3,4-dichlorophenylisothiocyanate (0.0031 mol) and the mixture was stirred at room temperature for 12 h. Then solvent was removed on rotary evaporator. The

reaction mixture was purified by column chromatography (chloroform: methanol; 9.5:0.5 vol.). Yield 71%, white powder, m.p. 156.5-158.5°C [1]. The IR spectrum (Fig.1) was obtained on Perkin Elmer Spectrum 1000 spectrometer in KBr pellets. FT-Raman spectrum (Fig. 2) was obtained on a Nicolet 6700 FT-IR Spectrometer with NXR FT-Raman Module, solid sample, Ge detector, excitation wavelength: 1064 nm, power at sample: maximum 150 mW, resolution: 2.0 cm^{-1}, number of scans: 1064. NMR spectra (^{1}H and ^{13}C) for the compound were recorded on a 500MHz NMR Spectrometer (Bruker advance, Reinstetten, Germany) using deuteriated DMSO and methanol as the solvent. The chemical shift values (ppm) and coupling constants (J) are given in δ and Hz respectively.

^{1}H NMR (300 MHz, DMSO) *δ*: 10.2 (br.s, 2H, NH), 7.9 (s, 1H), 7.9 (d, 1H, *J* =2.4 Hz), 7.7 (d, *J* = 8.1 Hz, 1H), 7.6-7.6 (m, 2H), 7.5-7.4 (m, 2H). ^{13}C NMR (75.4 MHz, DMSO) *δ*: 179.9 (C=S), 140.1, 139.4, 130.6, 130.3, 129.6, 129.1 (q, *J* = 31.8 Hz), 127.5, 126.4, 125.0, 124.0 (q, *J* = 272.1 Hz), 123.8, 121.0 (q, *J* = 3.8 Hz), 120.0 (q, *J* = 4.0 Hz). HRMS (ESI) calc. for $C_{14}H_8Cl_2F_3N_2S$ $[M-H]^-$: 362.9737, found: 362.9729.

3. Computational details

In this work for theoretical investigation of fundamental and local reactivity properties of title molecule we have used the lowest energy conformation as obtained after detailed conformational analysis. Initially, conformational analysis with MacroModel program as implemented in Schrödinger Materials Science Suite 2015-4 [27] yielded 95 different structures. All of these 95 structures have been initially optimized at B3LYP/6-31G(d) level of theory with Jaguar 9.0 program [28] program, also as implemented in Schrödinger Materials Science Suite 2015-4. Of these 95 structures five structures with the lowest energies have been chosen for more detailed optimization at B3LYP/6-31G(d,p) level of theory and with increased integral accuracy. Vibrational analysis has also been conducted in case of these five structures, to assure that true ground states are obtained. Finally, the lowest energy conformation has been chosen for further investigations. The NLO analysis, NBO analysis, frontier molecular orbital analysis and MEP are done with the help of Gaussian software [29, 30] and Gaussview software [31]. The GAR2PED software [32] is adapted to read the outputs from the program Jaguar and the potential energy distribution is calculated for the normal modes of vibrations of the title compound. A scaling factor value of 0.9613 is applied for the theoretically obtained wave number to get better agreement with the experimental wavenumbers [30].

Further, Jaguar 9.0 program has been used for DFT calculations of average local ionization energy (ALIE) surfaces, Fukui functions and BDE. B3LYP exchange-correlation

functional [33] has been used in all cases, with 6-311++G(d,p) basis set for ALIE surface, 6-31+G(d) for Fukui functions and 6-311G(d,p) for BDE. MD simulations have been performed with Desmond [34-37] program, also as implemented in Schrödinger Materials Science Suite 2015-4. OPLS 2005 force field [38] has been used within NPT ensemble class. Simulation time was 10 ns, while solvent was treated with simple point charge (SPC) model [39]. For calculation of charge transfer rates half of all possible pairs (around 60) of ANF-6 molecules were obtained from the last snapshot of MD simulation which was conducted under the same conditions. Such amorphous phase was modeled by placing the 32 ANF-6 molecules into the cubic box and simulating for 10 ns. Finally, the average value of charge transfer rates of electrons and holes was taken and it was compared with the values obtained for urea and thiourea molecules. Amorphous phases of urea and thiourea were obtained in the same way, with the difference that 256 molecules were placed in cubic box, because these molecules are much smaller than ANF-6.

4. Results and discussion

In the following discussion the tri-substituted and 1,3-disubstituted phenyl rings are designated as PhI and PhII, respectively.

4.1 Geometrical Parameters

Structures of five lowest energy conformers of ANF-6 molecule after geometrical optimization have been presented in Fig.3, while energies of mentioned conformers have been presented in Table 1, together with energy differences compared with the energy of the lowest energy conformer. According to the results presented in Table 1 the lowest energy structure of all possible conformations of ANF-6 molecule is the one denoted with ANF-6-34. Therefore, this structure is used for further detailed study of reactive, spectroscopic, transport and docking study. We will refer to this structure as ANF-6 and the labeled diagram is given in Fig.4 and the optimized geometrical parameters are given in Table S1 (supporting information).

The conformation around the thiourea bond is usually characterized by the syn/anti forms. Close inspection of molecular structures presented in Fig.3 indicate the lowest energy conformers of title molecule correspond to the anti-like forms. Among all 95 structures obtained by conformational search by MacroModel we have also chosen to present five lowest energy conformers of the syn form presented in Fig.S1 of the supplementary materials. It can be seen that syn forms are of tweezed molecule shape. Supplementary materials also contain potential energy scan around typical bond for thiourea derivatives, Fig. S2. Appropriate dihedral angle has been indicated in Fig.S3 of the supplementary materials.

The C-C bond lengths in the benzene rings are in the ranges 1.4035-1.3907 Å for PhI and 1.4006-1.3926 Å for PhII and these values are in between the normal values for a single and double bond (1.54 Å and 1.33 Å) [40]. For the title compound, the C-Cl bond lengths are 1.742 and 1.7448 Å which are in agreement with the reported values are 1.7550, 1.7595 Å (DFT), 1.7319, 1.7361 Å (XRD) [41].The CF_3 bond lengths of the title compound are 1.3543, 1.3522, 1.3502 Å and Mary et al. reported the CF_3 bond lengths as 1.3518-1.3642 Å (DFT), 1.3543-1.3607 Å (XRD) [42]. For the title compound, the C-C-F and F-C-F angles are 111.5, 112.0, 111.8° and 106.8° respectively while the reported values in the range 112.6-111.8° (DFT), 111.8-111.1° (XRD) and 106.0-107.2° (DFT), 101.8-109.7° (XRD) [42]. For the title compound, the C-N bond lengths are 1.4137, 1.3669, 1.3804 and 1.4135 Å while the reported values are 1.38, 1.404 Å [40] and 1.3814 Å [43] and the C-N bond lengths of the title compound are shorter than the C-N single bond of 1.4725 Å. The partial double bond character of the thiourea is due to the fact that the hydrogen bond locking the molecule into a planar six numbered ring structure [43]. For the title compound, the C-S bond length is 1.6750 Å and this lies between the values of C-S single and double bonds and the reported value is 1.6636 Å [43].

The bond angles around C_{15} and C_{14} positions, respectively, C_{14}-C_{15}-C_{16} = 120.1°, C_{14}-C_{15}-Cl_{17} = 121.4°, C_{16}-C_{15}-Cl_{17} = 118.5° and C_{13}-C_{14}-C_{15}= 119.2°, C_{13}-C_{14}-Cl_{18} = 119.1°, C_{15}-C_{14}-Cl_{18} =121.7° and the asymmetry in the values of angles is due to the presence of electronegative chlorine atoms. Due to the thiorea moeity there is an asymmetry for the bond angle values at C_{11} and C_2 positions, which are respectively, C_{12}-C_{11}-C_{16} = 119.2°, C_{12}-C_{11}-N_{10} = 122.4°, C_{16}-C_{11}-N_{10} = 118.2° and C_1-C_2-C_3 = 119.6°, C_1-C_2-N_7 = 123.6°, C_3-C_2-N_7 = 116.7°. The interaction between the phenyl rings and the thiourea moiety is evident from the asymmetry of the bond angles at the C_8 position and the angles are N_7-C_8-N_{10} = 114.0°, N_7-C_8-S_9 =127.1°, N_{10}-C_8-S_9 =118.9°. Due to the CF_3 group, the exocyclic angles at the position C_4 are C_3-C_4-C_{19} = 119.6° and C_5-C_4-C_{19} =119.8°. The thiourea moeity is tilted from the phenyl rings, as is evident from the torsion angles, C_3-C_2-N_7-C_8 = 152.0°, C_1-C_2-N_7-C_8 = -31.2°, C_{12}-C_{11}-N_{10}-C_8 = -42.3°, C_{16}-C_{11}-N_{10}-C_8 = 140.1°.

4.2 IR and Raman spectra

Table 2 contains calculated scaled wave numbers, observed IR, Raman bands and assignments of the title compound. According to the literature data the NH stretching and deformation modes are expected in the regions 3330-3450 cm^{-1} and 1400-1500, 450-600 cm^{-1} [44] and for the title compound, the NH stretching modes are observed at 3420, 3434 cm^{-1} in the IR spectrum, 3222 cm^{-1} in the Raman and at 3478, 3434 cm^{-1} theoretically. The

experimental NH stretching wavenumber is downshifted from the theoretical wavenumber and this is due to the intermolecular interaction. In the case of a thiourea derivative, Saeed et al. [45] reported the NH stretching modes at 3324, 3246, 3114 cm^{-1} in the IR spectrum and the corresponding theoretical wavenumbers are 3453, 3453, 3350 cm^{-1} and the downshift of the NH wavenumbers is due to the intermolecular interactions. For the title compound, the deformation modes of the NH groups are observed at 1532, 1470 cm^{-1} in the IR spectrum, 1528, 1471 cm^{-1} in the Raman spectrum and at 1529, 1470, 533, 505 cm^{-1} theoretically which are in agreement with the reported values [45-47].

In the present case the band at 728 cm^{-1} in the IR spectrum, 729 cm^{-1} in the Raman spectrum and 728 cm^{-1} theoretically is assigned as the CS stretching mode which is expected in the region 800 ± 130 cm^{-1} [44, 48, 49]. But higher wavenumber values upto 1100 cm^{-1} is also reported [50,51]. The C=S stretching modes are reported at 847, 835 cm^{-1} by Nigam et al. [52], at 908 cm^{-1} by Panicker et al. [43], in the range 796-693 cm^{-1} [53], 847, 739 cm^{-1} (DFT), 846, 732 cm^{-1} (Raman) [47], 801 cm^{-1} (IR), 798 cm^{-1} (Raman), 780 cm^{-1} (DFT) [45], 728 cm^{-1} (IR), 743, 698 cm^{-1} (DFT) [46] and at 733 cm^{-1} (IR), 742 cm^{-1} (DFT) [54].

For the title compound, CCl stretching modes are observed at 656, 684 cm^{-1} in the IR spectrum, 658, 688 cm^{-1} in the Raman spectrum and theoretically at 654, 688 cm^{-1} which is expected in the region 850-550 cm^{-1} [55]. The reported values of C-Cl stretching modes are 670 cm^{-1} (IR), 663 cm^{-1} (Raman) and 665 cm^{-1} (DFT) [56].

According to the literature, the CF_3 stretching modes are expected in the regions, 1300-1100 cm^{-1} and in-plane and out-of-plane bending modes in the regions, 720-440, 470-260 cm^{-1} [44] and in the present case, the bands at 1040 cm^{-1} in the IR spectrum, 1140 cm^{-1} in the Raman spectrum and at 1170, 1140, 1056 cm^{-1} theoretically are assigned as the CF_3 stretching modes. The reported values of CF_3 stretching modes are 1174, 1126, 1052 cm^{-1} [56] and 1140, 1026 cm^{-1} (IR), 1142, 1026 cm^{-1} (Raman), 1132, 1026, 1017 cm^{-1} (DFT) [57]. For the title compound, the CF_3 deformation modes are assigned at 553 cm^{-1} in the IR spectrum, 672, 553, 386, 350 cm^{-1} in the Raman spectrum and at 670, 556, 493, 389, 346 cm^{-1} theoretically which are in agreement with the reported values, at 550, 478 cm^{-1} (IR), 575, 394 cm^{-1} (Raman), 605, 574, 544, 486, 391, 389 cm^{-1} (DFT) [56], 674, 594, 511, 478 cm^{-1} (IR), 672, 601, 520, 475, 395, 372 cm^{-1} (DFT) [57] and at 678, 505 cm^{-1} (IR), 678, 498 cm^{-1} (Raman) and 684, 536, 502, 382, 374 and 313 cm^{-1} (DFT) [42]. For the title compound, the C-N stretching modes are assigned at 1188 cm^{-1} in the IR spectrum, 1203 cm^{-1} in the Raman spectrum and 1304, 1223, 1152, 1195 cm^{-1} theoretically which is in agreement with literature [43].

In the present case, the ring stretching modes of the phenyl rings are assigned at 1572, 1455, 1385, 1290 cm^{-1} (IR), 1582, 1550, 1451, 1381, 1286 cm^{-1} (Raman), 1579, 1548, 1456, 1379, 1285 cm^{-1} (DFT) for PhI and 1592, 1325 cm^{-1} (IR), 1603, 1483, 1420, 1325 cm^{-1} (Raman), 1606, 1592, 1481, 1411, 1327 cm^{-1} (DFT) for PhII which are in agreement with literature [44]. The ring breathing mode of the 1,3-disubstituted phenyl ring of the title compound is observed at 977 cm^{-1} in the Raman spectrum and at 980 cm^{-1} theoretically which is expected near 1000 cm^{-1} according to the literature [44, 58] and the reported value of the ring breathing mode is 1012 cm^{-1} [59]. In the case of tri-substituted benzenes, with mixed substituent, the ring breathing mode is expected in the range 600-750 cm^{-1} for mixed substituent, 500-600 cm^{-1} for light substituents and 1050-1100 cm^{-1} for mixed substituents [58] and in the present case, the band observed at 1099 cm^{-1} experimentally and at 1109 cm^{-1} (DFT) is assigned as the ring breathing mode of the tri-substituted phenyl ring. Madhavan et al. [60] reported this ring breathing mode at 1110, 1083 cm^{-1} theoreritcally and accoridng to Bhagyasree et al. [61] this mode is assigned at 1100 cm^{-1} (DFT), 1109 cm^{-1} (IR).

4.3 NMR Spectra

GIAO ^{1}H and ^{13}C NMR chemical shifts with respect to trimethylsilane were calculated using the DFT/B3LYP method (Table S2-supporting information) and compared with the experimental data. The experimental chemical shifts of aromatic protons of the title compound are in the range 7.4-7.6 for PhI and 7.5-7.9 for PhII while the calculated values are in the ranges, 7.2-7.7 for PhI and 7.0-8.9 for PhII. The hydrogen atoms of amide groups in this compound appear at a higher chemical shift of 10.2 ppm experimentally while δ_{calc} of the NH protons strongly deviate from the experimental data due to the high polarity of these bonds with values 7.0 and 6.9 ppm. For organic molecules, the range for ^{13}C NMR chemical shift is usually greater than 100 ppm [62], the accuracy ensures reliable interpretation of spectroscopic parameters. The aromatic carbons give resonance in overlapped areas of NMR spectrum with chemical shift values from 100 to 150 ppm [63] and in the present case, the experimental chemical shifts of the aromatic carbon atoms are, 123.8-139.4 PhI and 120.0-140.1 for PhII while the computed values are in the range, 120.0-144.7 for PhI and 118.7-138.6 for PhII. The chemical shifts of the other carbon atoms C8 and C19 are 177.8 (computed), 179.9 (experimental) and 133.5 (computed), 124.0 ppm (experimental).

4.4 Frontier Molecular Orbital analysis

The HOMO, LUMO energies and the HOMO-LUMO energy gap of organic molecules are significant because of they relate to specific movements of electrons and may be most important for single electron transfer. This is useful for a number of reactions, and

has huge implications in organic semiconductors. If the HOMO-LUMO gap is large, the molecules are highly stable and unreactive, while those with small gaps are generally reactive [64]. Using the HOMO-LUMO gap one can easily determine the excitation energy of oraganic derivative at its ground state [65]. The HOMO-LUMO plots are given in Fig.5. From Fig. 5 it is clear that, the HOMO is all over the molecule except the CF_3 group and LUMO is over the phenyl ring PhII, CF_3 group and CS group. The HOMO, LUMO energies and the energy gap are respectively, -7.319, -4.549 and 2.77 eV. The ionization energy and electron affinity can be expressed as: $I = -E_{HOMO} = 7.319$, $A = -E_{LUMO} = 4.549$ eV [66]. The hardness η and chemical potential μ are given the following relations $\eta = (I-A)/2$ and $\mu = -(I+A)/2$, where I and A are the first ionization potential and electron affinity of the chemical species [67]. For the title compound, the chemical descriptors are, ionization potential, I = 7.319 eV, electron affinity A= 4.549 eV, global hardness η = 1.385 eV, chemical potential μ = -5.934 eV, global electrophiliciy index $= \mu^2/2\eta = 12.712$ eV.

4.5 Molecular Electrostatic Potential

MEP map gives three dimensional view of charge distribution and the reactive sites of the molecule. The interactions between the molecules and the physiochemical property relationships can be studied by using the MEP map [68-71]. The different values of the electrostatic potential at the MEP plot are given by different colors with potential values increases in the order red < orange < yellow < green < blue. The red, orange and yellow regions of the MEP (Fig.6) are negative potential regions related to electrophilic reactivity. The maximum negative region is localized over the C=S group and 1,3-disubstituted phenyl ring and the maximum positive region is localized on NH groups indicating a possible site for nucleophilic attack. These sites give the most reactive sites for both electrophilic and nucleophilic attack.

4.6 ALIE surfaces, Fukui functions and intra-molecular non-covalent interactions

ALIE as quantum molecular descriptor was introduced by Sjoberg et al. [72, 73] to describe the reactivity properties of aromatic molecular systems. It is defined as sum of orbital energies weighted by the orbital densities according to the following equation:

$$I(r) = \sum_i \frac{\rho_i(\vec{r})|\varepsilon_i|}{\rho(\vec{r})}, \quad (1)$$

where $\rho_i(\vec{r})$ represents the electronic density of the *i*-th molecular orbital at the point $\vec{r}$, ε_i represents the orbital energy and $\rho(\vec{r})$ is the total electronic density function. When ALIE is mapped to the electron density surface it indicates molecule areas where electrons are least

tightly bound and therefore the locations where electrophilic attacks could be the most effective.

ALIE surface presented in Fig.7 clearly indicates that the sulfur atom is location possibly prone to the electrophilic attacks as significant amount of red color is located precisely there. In other words, here the electrons are the most easily removed. Red color of ALIE surface in the case of ANF-6 molecule denotes that somewhat more than 165 kcal/mol is needed for the removal of electrons in the near vicinity of sulfur atom. As already pointed out, the possibility of thiourea compounds to form intra and intermolecular noncovalent interactions is very important [19, 45, 47, 74]. In this particular example, sulfur atom is important from the aspect of intramolecular noncovalent interactions. Namely, only one such interaction has been detected and it involves sulfur atom and hydrogen atom H23.

Important reactive centers were also detected by calculation of Fukui functions. This quantum molecular descriptor represents the measure of electron density that is gained/lost as a consequence of charge addition/removal. In Jaguar program Fukui f^+ and f^- functions are calculated in finite difference approximation via following equations:

$$f^+ = \frac{\left(\rho^{N+\delta}(r) - \rho^N(r)\right)}{\delta}, \tag{2}$$

$$f^- = \frac{\left(\rho^{N-\delta}(r) - \rho^N(r)\right)}{\delta}, \tag{3}$$

where N denotes the number of electrons in the reference state of the molecule and δ represents the fraction of electron, which is set to be 0.01 [75]. The values of Fukui functions are mapped to the electron density surface and the representative ones are presented in Fig.8. In Fig.8a purple color denotes locations with positive values of Fukui f^+ function and therefore locations within ANF-6 molecule where electron density increases when charge is added. It can be seen that there are three specific locations where purple color is localized, carbon atom C13, hydrogen atom H31 and sulfur atom S9. In Fig.8b red color denotes locations with negative values Fukui f^- function and therefore locations within ANF-6 molecule where electron density decreases when charge is removed. The distribution of red color indicates that much larger area of ANF-6 molecule is reduced in terms of electron density as a consequence of charge removal.

4.7 NBO Analysis

The natural bond orbitals (NBO) calculations were performed using NBO 3.1 program [76] as implemented in the Gaussian09 package at the DFT/B3LYP level and the important results are tabulated in Tables S3 and S4 (supporting information). The intra-

molecular hyper conjugative interactions in the molecular system are: C_8-S_9 from N_7 of $n_1(N_7)\rightarrow\sigma^*(C_8\text{-}S_9)$ which increases the electron density 0.48071e and weakens the respective bonds C_8-S_9 leading to stabilization of 68.14 kJ/mol; C_8-S_9 from N_{10} of $n_1(N_{10})\rightarrow\sigma^*(C_8\text{-}S_9)$ which increases the electron density 0.48071e and weakens the respective bonds C_8-S_9 leading to stabilization of 66.19 kJ/mol; C_{14}-C_{15} from Cl_{17} of $n_3(Cl_{17})\rightarrow\pi^*(C_{14}\text{-}C_{15})$ which increases the electron density 0.46303e and weakens the respective bonds C_{14}-C_{15} leading to stabilization of 14.24 kJ/mol; C_{14}-C_{15} from Cl_{18} of $n_3(Cl_{18})\rightarrow\pi^*(C_{14}\text{-}C_{15})$ which increases the electron density 0.46303e and weakens the respective bonds C_{14}-C_{15} leading to stabilization of 13.90 kJ/mol; C_{19}-F_{21} from F_{20} of $n_3(F_{20})\rightarrow\sigma^*(C_{19}\text{-}F_{21})$ which increases the electron density 0.10271e and weakens the respective bonds C_{19}-F_{21} leading to stabilization of 11.46 kJ/mol; C_{19}-F_{22} from F_{21} of $n_3(F_{21})\rightarrow\sigma^*(C_{19}\text{-}F_{22})$ which increases the electron density 0.10285e and weakens the respective bonds C_{19}-F_{22} leading to stabilization of 12.84 kJ/mol; C_{19}-F_{21} from F_{22} of $n_3(F_{22})\rightarrow\sigma^*(C_{19}\text{-}F_{21})$ which increases the electron density 0.10271e and weakens the respective bonds C_{19}-F_{21} leading to stabilization of 12.87 kJ/mol. The natural hybrid orbital with higher energies, considerable p-characters (100%) and low occupation numbers are $n_2(S_9)$, $n_3(Cl_{17})$, $n_3(F_{18})$, $n_3(F_{20})$, $n_3(F_{21})$, and $n_3(F_{22})$. The energies and occupation numbers of these orbitals are -0.19884, -0.33765, -0.42637, -0.42376, -0.41733, -0.42439 a.u. and 1.87411, 1.92492, 1.91319, 1.93051, 1.93139, 1.93148. The orbital with lower energies and high occupation numbers are $n_1(Cl_{17})$, $n_1(S_9)$, $n_1(F_{18})$, $n_1(F_{20})$, $n_1(F_{21})$ and $n_1(F_{22})$. The energies, p-characters and occupation numbers of these orbital are respectively, -0.93461, -0.69927, -1.04846, -1.05905, -1.05996, -1.06075 a.u. and 17.66, 17.93, 30.30, 29.17, 99.98, 29.05% and 1.99362, 1.98601, 1.98857, 1.98707, 1.98756, 1.98711. Thus, a very close to pure p-type lone pair orbital participates in the electron donation to the $n_1(N_7)\rightarrow\sigma^*(C_8\text{-}S_9)$, $n_2(S_9)\rightarrow\sigma^*(N_7\text{-}C_8)$, $n_1(N_{10})\rightarrow\sigma^*(C_8\text{-}S_9)$,and $n_3(Cl_{17})\rightarrow\pi^*(C_{14}\text{-}C_{15})$ interactions in the compound as reported in literatue [74, 77].

4.8 Nonlinear Optical Properties

For the title compound, the polarizability, first hyperpolarizability and second hyperpolarizability are respectively, 3.186×10^{-23}, 5.0295×10^{-30} and -26.568×10^{-37} esu and these values of the investigated molecule clearly reveal that they have nonlinear optical behavior with non-zero values. The reported value of the first hyperpolarizability of phenyl thiourea derivatives is 1.86×10^{-30} esu [43] and the first hyperpolarizability of the title compound is 38.69 times that of the standard NLO material urea [78].

4.9 Degradation properties based on the autoxidation and hydrolysis

Stability and degradation properties of newly synthetized biologically active molecules are of great importance for the practical applications [79, 80]. Stability is important prerequisite for the application of PCCPs, which are known to be very stable. On the other side high stability of PCCPs hardens the process of water purification, because conventional procedures are neither suitable nor economic for their removal. In order to improve the present and develop new purification procedures it is necessary to understand in details the reactive and degradation properties of biologically active molecules.

Two mechanisms are of particular importance for the degradation – autoxidation and hydrolysis. Both of these processes can be inexpensively investigated employing the DFT calculations and MD simulations. For the investigation of autoxidation possibilities calculation of BDE can be particularly useful. Namely, if the BDE for hydrogen abstraction at some location of molecule is in certain energy interval than that position can be considered as potentially available for the start of autoxidation. According to the study of Wright et al. [81] the molecule is the most sensitive towards autoxidation if the BDE for hydrogen abstraction is in the interval between 75–85 kcal/mol. On the other side, it is known that formation of radical of organic biologically active molecule occurs with formation of peroxy radical. Further reaction can be possible if the formed peroxy radical is able to abstract hydrogen atom from another molecule [80]. All peroxy radicals are having BDEs in the range of 87–92 kcal/mol, so these values should be also taken into account concerning the prediction of possible locations suitable for the start of autoxidation [80, 82]. Beside BDEs for hydrogen abstraction, knowing the BDEs for the rest of the single acyclic bonds is also very useful because weakest bonds can be located. BDEs for all single acyclic bonds are presented in Fig.9. In Fig.9 it can be seen that only one BDE value for hydrogen abstraction (bond denoted with number 5) is just below 92 kcal/mol. This is however on the upper border level and it is hard to expect that this location is suitable for the start of autoxidation. On the other side two locations with the lowest BDEs are bonds denoted with numbers 12 and 13. In these cases BDEs are having values below 70 kcal/mol and indicate that these are the locations where degradation could start. It is also important to notice that these bonds are in the near vicinity of sulfur atom, which is important reactive center according to ALIE and Fukui function surfaces.

Spatial distribution of solvent molecules provides important information on the interactions of certain atoms with solvent. In this regard, RDF, $g(r)$, is the quantity that indicates the probability of finding a particle in the distance r from another particle [83]. RDF curves of atoms that have pronounced interactions with water are given in Fig.10. Fig.10a

contains RDFs of carbon atoms. It can be seen that there are five carbon atoms with significant interactions with water molecules, among which the highest g(r) value, almost 1.4, has been calculated for carbon atom C19, while its peak distance is located at around 4 Å. From the aspect of RDF profile carbon atoms C6, C12 and C13 are very similar, with C6 having the highest g(r) value and with C12 having the shortest peak distance. The highest g(r) value of carbon atom C4 is located at around 1.2, while its peak distance is located at around 5 Å. Fig.10b contains RDFs of non-carbon atoms with pronounced interactions with water molecules. Certainly the most important atom from the aspect of interactions with water molecules is hydrogen atom H28 which has g(r) value of almost 0.8 and peak distance that is lower than 2 Å. Sulfur and chlorine atoms are very similar regarding the profile of RDF. The highest g(r) values are around 1.3, while peak distance is located at around 3.5 Å. Thus, sulfur atom and hydrogen atom H28 are determined as significant reactive center by RDFs. These facts are important as the weakest bonds (bonds 12 and 13 as denoted in Fig. 9) are located in the near vicinity of mentioned atoms indicating that degradation could start here.

4.10 Charge transfer rates between ANF-molecules

Among many fantastic properties thiourea derivatives also have potential to be applied as phase change materials [84]. This class of materials has great potential when it comes to the areas of solar energy storage, waster heat recovery, smart air-conditioned buildings, temperature-adaptable greenhouses, electric appliances with thermostatic regulators, etc. Besides, certain thiourea derivatives have been considered as new OLED materials [20, 85, 86]. This has motivatived us to investigate transport properties of the title molecule using the Marcus semi-empiric approach. According to the Marcus semi-empiric approach charge transfer rates of electrons and holes, k_{ET} , are given by the following expression [87, 88]:

$$k_{ET} = \frac{4\pi^2}{h} \frac{1}{\sqrt{4\pi\lambda k_B T}} t^2 \exp\left[\frac{-\lambda}{4k_B T}\right]. \quad (4)$$

where λ is reorganization energies (λ_- for electrons and λ_+ for holes), while *t* isthe transfer integral. k_{ET} is directly proportional to the mobility of charge carriers and diffusion coefficient so its calculation provides important electronic properties of some molecule. It can be seen by brief analysis of equation (4) that in order to achieve the maximal values of k_{ET}, reorganization energies should be minimal, while charge coupling should be maximized. Calculated optoelectronic properties have been presented in Table 3. Once the possible pairs of ANF-6 molecules were obtained by MD simulations, calculations of *t* have been performed for 60 randomly chosen pairs (half of the total number of pairs) and the average values have

been taken. Same procedure was conducted for obtaining charge hopping rates for urea and thiourea molecules. According to the results presented in Table 3 electron reorganization energy of ANF-6 molecule is significantly lower than of urea and thiourea molecules, while hole reorganization energy is higher. On the other side transfer integrals in case of ANF-6 are much lower. Such combination of parameters important for charge transfer rates produces better results in the case of electrons. Namely, charge transfer rates of electrons are one order of magnitude better in case of ANF-6 comparing with urea and thiourea molecules. On the other side higher reorganization energy of holes in the case of ANF-6 leads to the values of k_{ET}^{+} that are lower than in cases of urea and thiourea molecules. Not only that k_{ET}^{-} is better in the case of ANF-6, but thedifference between k_{ET}^{-} and k_{ET}^{+} is also very low, which is result that is important for the practical applications. Namely, it is necessary for k_{ET}^{-} and k_{ET}^{+} to be as high as possible, but if the difference between k_{ET}^{-} and k_{ET}^{+} is too large (several orders of magnitude), then recombination easily occurs. As provided in Table 3, k_{ET}^{-} and k_{ET}^{+} are of the same order of magnitude.

4.11 Molecular Docking

Based on the structure of a compound, PASS (Prediction of Activity Spectra) [89] is an online tool which predicts different types of activities. PASS analysis of the title compound predicts activities given in the Table 4, cytochrome reductase activity with probability to be active (Pa) value of 0.763.Cytochrome bc1 reductase against the antifungal agent ilicicolin H [90] and substituted aromatic and aliphatic thiourea compounds are antifungal agent [91, 92]. High resolution crystal structure of cytochrome reductase was downloaded from the RSCB protein data bank website with PDB ID: 1RIE and all molecular docking calculations were performed on Auto Dock-Vina software [93] and as reported earlier [55]. From the docked conformations [94], using Discovery Studio Visualizer 4.0 software, the one which binds well at the active site was analysed for detailed interactions. The weak non-covalent interactions and these interactions are depicted in Fig.11 and the interactions are: Amino acid Val182 forms interactions like H-bond, π-sigma and alkyl with phenyl ring and π-alkyl with CF_3 group. Lis128 shows H-bond and alkyl interaction with CF_3 group.Val127, Arg126 forms halogen interaction with CF_3 group. Glu125 exhibit H-bond with NH group and Tyr 185 forms π-alkyl interaction with CF_3 group. The docked ligand forms a stable complex with cytochrome reductase (Fig.12) and got a binding affinity value of -6.3 kcal/mol (Table 5). Thus the title compound can be a lead compound for developing new antifungal agent.

5. Conclusion

The vibrational wave numbers of the title compound have been assigned, analyzed and the theoretical wave numbers are compared with the experimental results. The theoretically predicted geometrical parameters are in agreement with that of similar derivatives. Frontier molecular orbital studies reveal the charge transfer through the conjugated system. The first and second hyperpolarizability values are reported. According to both ALIE and Fukui f^+ function values mapped to the electron density surface sulfur atom is possibly prone to the electrophilic attacks. Carbon atom C13 and hydrogen atom H31 could also be important reactive centers, as shown by the Fukui f^+ function. The only intramolecular noncovalent interaction was detected between sulfur atom S9 and hydrogen atom H23. Only one bond had BDE value for hydrogen abstraction lower than and very close to 92 kcal/mol, thus it is expected that title molecule is stable at open air and in the presence of oxygen. According to RDFs the most pronounced interactions with water molecule occurred in case of hydrogen atom H28, while sulfur atoms S9 also had significant RDF profile indicating interactions with water molecules. Since according to BDEs the weakest bonds are in the close vicinity of mentioned atoms, it is to be expected that degradation could start here. Charge transfer rates of electrons in case of ANF-6 molecules are significantly better than in case of urea and thiourea molecules. In the same time charge transfer rates of both electrons and holes are of same order of magnitude, which could be useful from the aspect of recombination. The non-covalent interactions obtained from the docking studies are: Amino acid Val182 forms interactions like H-bond, π-sigma and alkyl with phenyl ring and π-alkyl with CF_3 group; Lis128 shows H-bond and alkyl interaction with CF_3 group; Val127, Arg126 forms halogen interaction with CF_3 group; Glu125 exhibit H-bond with NH group and Tyr 185 forms π-alkyl interaction with CF_3 group.

Acknowledgements

Part of this work has been performed thanks to the support received from Schrödinger Inc. Part of this study was conducted within the projects supported by the Ministry of Education, Science and Technological Development of Serbia, grant numbers ON171039, TR34019. The authors are thankful to University of Antwerp for access to the University's CalcUA supercomputer cluster.

References

[1] A. Bielenica, J. Stefańska, K. Stępień, A. Napiórkowska, E. Augustynowicz-Kopeć,

G. Sanna, S. Madeddu, S. Boi, G. Giliberti, M. Wrzosek, M. Struga, Synthesis, cytotoxicity and antimicrobial activity of thiourea derivatives incorporating 3-(trifluoromethyl)phenyl moiety, Eur. J. Med. Chem. 101 (2015) 111-125.

[2] A. Bielenica, K. Stępień, A. Napiórkowska, E. Augustynowicz-Kopeć, S. Krukowski, M. Włodarczyk, M. Struga Synthesis and antimicrobial acitivity of 4-chloro-3-nitrophenylthiourea derivatives targeting bacterial type II topoisomerases, Chem. Biol. Drug Des. 87 (2016) 905-917.

[3] H.M. Faidallah, K.A. Khan, A.M. Asiri, Synthesis and biological evaluation of new 3-trifuloromethylpyrazolesulfonyl-urea and thiourea derivatives as antidiabetic and antimicrobial agents, J. Fluorine Chem. 132(2011) 131-137.

[4] H.M. Faidallah, S.A. Rostom, S.A. Basaif, M.S. Makki, K.A. Khan, Synthesis and biological evaluation of some novel urea and thiourea derivatives of isoxazolo(4,5-d)pyridazine and structurally related thiazolo(4,5-d)pyridazine as antimicrobial agents, Arch. Pharm. Res. 36 (2013) 1354-1368.

[5] A.P. Keche, G.D. Hatnapure, R. H. Tale, A.H. Rodge, S.S. Birajdar, V.M. Kamble, A novel pyrimidine derivatives with aryl urea, thiourea and sulfonamide moieties, synthesis, anti-inflammatory and antimicrobial evaluation, Bioorg. Med. Chem. Lett. 22 (2012) 3445-3448.

[6] D. Sriram, P.Yogeeswari, M. Dinakaran, R. Thirumurugan, Antimycobacterial activity of novel 1-(5-cyclobutyl-1,3-oxazol-2-yl)-3-(sub)phenyl/pyridylthiourea compounds endowed with high activity toward multidrug resistant mycobacterium tuberculosis, J. Antimicrob.Chemother. 59 (2007) 1194-1196.

[7] R.M. Kumbhare, T. Dadmal, U. Kosurkar, V. Sridhar, J.V. Rao, Synthesis and cytotoxic evaluation of thiourea and N-bis-benzothiazole derivatives, a novel class of cytotoxic agents, Bioorg. Med. Chem. Lett. 22 (2012) 453-455.

[8] T. Stringer, D. Taylor, C. de Kock, H. Guzgay, A. Au, S.H. An, B. Sanchez, R. O'Connor, N. Patel, K.M. Land, P.J. Smith, D.T. Hendricks, T.J. Egan, G.S. Smith, Synthesis, characterization, antiparasitc and cytotoxic evaluation of thioureas conjugated to polyamine scaffolds, Eur. J. Med. Chem. 69 (2013) 90-98.

[9] İ. Koca, A. Özgür, K.A. Coşkun, Y. Tutar, Synthesis and anticancer activity of acyl thioureas bearing pyrazole moiety, Bioorg. Med. Chem. 21 (2013) 3859-3865.

[10] D.E. Ehmann, S.D. Lahiri, Novel compounds targeting bacterial DNA topoisomerase/DNA gyrase, Curr. Opin. Pharmacol. 18 (2014) 76-83.

[11] J. Stefanska, G. Nowicka, M. Struga, D. Szulczyk, A.E. Koziol, E. Augustynowicz-

Kopec, A. Napiorkowska, A. Bielenica, W. Filipowski, A. Filipowska, A. Drzewiecka, G. Giliberti, S. Madeddu, S. Boi, P. La Colla, G. Sanna, Antimicrobial and anti-biofilm activity of thiourea derivatives incorporating a 2-aminothiazole scaffold, Chem. Pharm. Bull. (Tokyo) 63 (2015) 225-236.

[12] S.Y. Abbas, M.A.M. El-Sharief, W.M. Basyouni, I.M. Fakhr, E.W. El-Gammal, Thiourea derivatives incorporating a hippuric acid moiety, synthesis and evaluation of antibacterial and antifungal activities, Eur. J. Med. Chem. 64 (2013) 111-120.

[13] J.M. Vega-Pérez, I. Periñán, M. Argandoña, M. Vega-Holm, C. Palo-Nieto, E. Burgos-Morón, M. López-Lázaro, C. Vargas, J. J. Nieto, F. Iglesias-Guerra, Isoprenyl thiourea and urea derivatives as a new farnesyl diphosphate analogues, synthesis and in viro antimicrobial and cytotoxic activities, Eur. J. Med. Chem. 58 (2012) 591-612.

[14] K.M. Khan, F. Naz, M. Taha, A. Khan, S. Perveen, M.I. Choudhary, W. Voelter, Synthesis and in vitro urease inhibitory activity of N,N'-disubstituted thioureas, Eur. J. Med. Chem. 74 (2014) 314-323.

[15] M.K. Rauf, A. Talib, A. Badshah, S. Zaib, K. Shoaib, M. Shahid, U. Flörke, I.-ud-Din, J. Iqbal, Solution phase microwave assisted parallel synthesis of N,N'disubstituted thioureas derived from benzoic acid, biological evaluation and molecular docking studies, Eur. J. Med. Chem. 70 (2013) 487-496 .

[16] G. Koutoulogenis, N. Kaplaneris, C.G. Kokotos, (Thio) urea-mediated synthesis of functionalized six-membered rings with multiple chiral centers, Beilstein J. Org. Chem. 12(1) (2016) 462-495.

[17] A. Saeed, U. Florke, M.F. Erben, A review on the chemistry, coordination, structure and biological properties of 1-(acyl/aroyl)-3-(substituted) thioureas, J. Sulfur Chem. 35(3) (2014) 318-355.

[18] V.B. Bregović, N. Basarić, K. Minarić-Majerski, Anion binding with urea and thiourea derivatives, Coord. Chem. Rev. 295 (2015) 80-124.

[19] H.-L. Chen, Z.-F. Guo, Z.-I. Lu, Controlling ion-sensing specificity of N-amidothiourea, From anion-selective sensors to highly Zn2+ -selective sensors by tuning electronic effects, Org. Lett. 14(19) (2012) 5070-5073.

[20] S.M. Jasman, W.M. Khairul, T. Tagg, K. KuBulat, R. Rahamathullah, S. Arshad, I.A. Razad, M.I.M. Tahir, Synthesis, crystal structure and electrical studies of naphthoyl-thiourea as potential organic light emitting diode, J. Chem. Cryst. 45(7) (2015) 338-349.

[21] A. Golubović, B. Abramović, M. Šćepanović, M. Grujić-Brojčin, S. Armaković, I. Veljković, B. Babić, Z. Dohčević-Mitrović, Z. Popović, Improved efficiency of sol-gel synthesized mesoporous anatase nanopowders in photocatalytic degradation of metoprolol, Mater. Res. Bull. 48 (2013) 1363-1371.

[22] R. Ma, B. Wang, S.Lu, Y. Zhang, L. Yin, J. Huang, S. Deng, Y. Wang, G. Yu, Characterization of pharmaceutically active compounds in Dongiting Lake, China: Occurrence, chiral profiling and environmental risk, Sci. Total Environ. 557 (2016) 268-275.

[23] S.J. Armaković, S. Armaković, N.L. Finčur, F. Šibul, D. Vione, J.P. Šetrajčić, B. Abramović, Influence of electron acceptors on the kinetics of metoprolol photocatalytic degradation in TiO_2 suspension: A combined experimental and theoretical study, RSC Advances 5 (2015) 54589-54604.

[24] B. Abramović, S. Kler, D. Šojić, M. Laušević, T. Radović, D. Vione, Photocatalytic degradation of metoprolol tartrate in suspensions of two TiO2-based photocatalysts with different surface area. Identification of intermediates and proposal of degradation pathways, J. Hazard. Mater. 198 (2011) 123-132.

[25] J.J. Molnar, J.R. Agbaba, B.D. Dalmacija, M.T. Klašnja, M.B. Dalmacija, M.M. Kragulj, A comparitive study of the effects of ozonation and TiO_2 catalzed ozonation on the selected chlorine disinfection by product precursor content and structure, Sci. Total Environ. 425 (2012) 169-175.

[26] J. Molnar, J. Agbaba, B. Dalmacija, M. Klašnja, M. Watson, M. Kragulj, Effects of ozonation and catalytic ozonation on the removal of natural organic matter from groundwater, J. Environ. Engineering 138 (2011) 804-808.

[27] Materials Science Suite 2015-4, Schrödinger, LLC, New York, NY, 2015.

[28] A.D. Bochevarov, E. Harder, T.F. Hughes, J.R. Greenwood, D.A. Braden, D.M. Philipp, D. Rinaldo, M.D. Halls, J. Zhang, R.A. Friesner, Jaguar: A High performance Quantum Chemistry Software Program with Strengths in Life and Materials Sciences, Int. J. Quantum Chem. 113 (2013) 2110-2142.

[29] Gaussian 09, Revision B.01, M.J. Frisch, G.W. Trucks, H.B. Schlegel, G.E. Scuseria, M.A. Robb, J.R. Cheeseman, G. Scalmani, V. Barone, B. Mennucci, G.A. Petersson, H. Nakatsuji, M. Caricato, X. Li, H.P. Hratchian, A.F. Izmaylov, J. Bloino, G. Zheng, J.L. Sonnenberg, M. Hada, M. Ehara, K. Toyota, R. Fukuda, J. Hasegawa, M. Ishida, T. Nakajima, Y. Honda, O. Kitao, H. Nakai, T. Vreven, J.A. Montgomery, Jr., J.E. Peralta, F. Ogliaro, M. Bearpark, J.J. Heyd, E. Brothers, K.N. Kudin, V.N. Staroverov,

T. Keith, R. Kobayashi, J. Normand, K. Raghavachari, A. Rendell, J.C. Burant, S.S. Iyengar, J. Tomasi, M. Cossi, N. Rega, J.M. Millam, M. Klene, J.E. Knox, J.B. Cross, V. Bakken, C. Adamo, J. Jaramillo, R. Gomperts, R.E. Stratmann, O. Yazyev, A.J. Austin, R. Cammi, C. Pomelli, J.W. Ochterski, R.L. Martin, K. Morokuma, V.G. Zakrzewski, G.A. Voth, P. Salvador, J.J. Dannenberg, S. Dapprich, A.D. Daniels, O. Farkas, J.B. Foresman, J.V. Ortiz, J. Cioslowski, D.J. Fox, Gaussian, Inc., Wallingford CT, 2010.

[30] J.B. Foresman, Pittsburg, PA, in: E. Frisch (Ed.). Exploring Chemistry with Electronic Structure Methods: A Guide to Using Gaussian, 1996.

[31] R. Dennington, T.Keith, J. Millam, Gaussview, Version 5, Semichem Inc., ShawneeMission, KS, 2009.

[32] R.M.L. Martin, C. Van Alsenoy, GAR2PED, a Program to Obtain a Potential Energy Distribution from a Gaussian Archive Record, University of Antwerp, Belgium, 2007.

[33] A.D. Becke, Density functional thermochemistry. III. The role of exact exchange, J. Chem. Phys. 98 (1993) 5648-5652.

[34] D. Shivakumar, J. Williams, Y. Wu, W. Damm, J. Shelley, W. Sherman, Prediction of absolute solvation free energies using molecular dynamics free energy perturbation and the OPLS force field, J. Chem. Theory Comput. 6 (2010) 1509-1519.

[35] Z. Guo, U. Mohanty, J. Noehre, T.K. Sawyer, W. Sherman, G. Krilov, Probing the α-helical structural stability of stapled p53 peptides: Molecular dynamics simulations and anlaysis, Chem. Biol. Drug Design 75 (2010) 348-359.

[36] K.J. Bowers, E. Chow, H. Xu, R.O. Dror, M.P. Eastwood, B.A. Gregersen, J.L. Klepeis, I. Kolossvary, M.A. Moraes, F.D. Sacerdoti. *Scalable algorithms for molecular dynamics simulations on commodity clusters*. in *SC 2006 Conference, Proceedings of the ACM/IEEE*. 2006. IEEE.

[37] *Schrödinger Release 2015-4: Desmond Molecular Dynamics System, version 4.4, D. E. Shaw Research, New York, NY, 2015. Maestro-Desmond Interoperability Tools, version 4.4, Schrödinger, New York, NY, 2015.* 2015.

[38] J.L. Banks, H.S. Beard, Y. Cao, A.E. Cho, W. Damm, R. Farid, A.K. Felts, T.A. Halgren, D.T. Mainz, J.R. Maple, R.Murphy, DM.Philipp, MP.Repasky, LY.Zhang, BJ.Berne, RA.Friesner, E.Gallicchio, RM.Lew, Integrated modeling program, applied chemical theory (IMPACT), J. Comput. Chem. 26 (2005) 1752-1780.

[39] H.J. Berendsen, J.P. Postma, W.F. van Gunsteren, J. Hermans, *Interaction models for water in relation to protein hydration*, in *Intermolecular forces*. 1981, Springer. p. 331-342.

[40] K.G.V. Das, C.Y. Panicker, B. Narayana, P.S. Nayak, B.K. Sarojini, FT-IR, molecular structure, first order hyperpolarizability, NBO analysis, HOMO and LUMO and MEP analysis of 1-(10H-phenothiazin-2-yl)ethanone by HF and density functional methods, Spectrochim. Acta 135 (2015) 162-171.

[41] Y.S. Mary, C.Y. Panicker, P.L. Anto, M. Sapnakumari, B. Narayana, B.K. Sarojini, Molecular structure, FT-IR, NBO, HOMO and LUMO, MEP and first order hyperpolarizability of (2E)-1-(2,4-dichlorophenyl)-3-(3,4,5-trimethoxyphenyl)prop-2-en-1-one by HF and density functional methods, Spectrochim. Acta 135 (2015) 81-92.

[42] Y.S. Mary, C.Y. Panicker, T.S. Yamuna, M.S. Siddegowda, H.S. Yathirajan, A.A. Al-Saadi, C. Van Alsenoy, Theoretical investigations on the molecular structure, vibrational spectra, HOMO-LUMO and NBO analysis of 9-[3-(dimethylamino) propyl]-2-trifluoro-methyl-9H-thioxanthen-9-ol, Spectrochim. Acta 132 (2014) 491-501.

[43] C.Y. Panicker, H.T. Varghese, A. George, P.K.V. Thomas, FT-IR, FT-Raman and ab initio studies of 1,3-diphenyl thiourea, Eur. J. Chem. 1 (2010) 173-178.

[44] N.P.G. Roeges, A Guide to the Complete Interpretation of Infrared Spectra of Organic Structures, John Wiley and Sons Inc., New York, 1994.

[45] A. Saeed, A. Khurshid, M. Bolte, A.C. Fantoni, M.F. Erben, Intra- and intermolecular hydrogen bonding and conformation in 1-acyl thioureas: An experimental and theoretical approach on 1-(2-chlorbenzoyl)thiourea, Spectrochim. Acta 143 (2015) 59-66.

[46] M. Mushtaque, M. Jahan, A. Ali, M.S. Khan, M.S. Khan, P. Sahay, A. Kesarwani, Synthesis, characterization, molecular docking, DNA binding, cytotoxicity and DFT studies of 1-(4-methoxyhenyl)-3-(pyridine-3-ylmethyl)thiourea, J. Mol. Struct. 1122 (2016) 164-172.

[47] A. Saeed, S. Ashraf, J.M. White, D.B. Soria, C.A. Franca, M.F. Erben, Synthesis, X-ray structure, thermal behaviour and spectroscopic anlaysis of 1-(1-naphthoyl)-3-(halo-phenyl)-thioureas complemented with quantum chemical calculations, Spectrochim. Acta A 150 (2015) 409-418.

[48] N.B. Colthup, L.H. Daly, S.E. Wiberly, Introduction of Infrared and Raman Spectroscopy, Academic Press, New York, 1975.

[49] G. Socrates, Infrared Characteristic Group Frequencies, John Wiley and Sons, New York, 1981.

[50] K. Srinivasan, S. Gunasekaran, S. Krishnan, Spectroscopic investigations and structural confirmation studies on thioures, Spectrochim. Acta A 75 (2010) 1171-1175.

[51] Z. Weiqun, L. Baolong, Z. Liming, D. Jiangang, Z. Yong, L. Lude, Y. Xujie, Structural and spectral studies on N-(4-chloro)benzoyl-N'-(4-tolyl)thiourea, J. Mol. Struct. 690 (2004) 145-150.

[52] S. Nigam, M.M. Patel, A. Ray, Normal coordinate analysis and CNDO/II calculations of isonitrosopropiohenone (propiophenone oxime) and its semicarbazone and thiosemicarbazone derivatives, synthesis and characterization of their metal complexes, J. Phys. Chem. Solids, 61 (2000) 1389-1398.

[53] O. Estevez-Hernandez, E. Otazo-Sanchez, J.L.H.H. de Cisneros, I. Naranjo-Rodriguez, E. Reguera, A Raman and infrared study of 1-furoyl-3-monosubstituted and 3,3-disubstituted thioureas, Spectrochim. Acta 62 (2005) 964-971.

[54] A. Saeed, S. Ashraf, U. Florke, Z.Y.D. Espinoza, M.F. Erben, H. Perez, Supramolecular self assembly of a coumarine based acylthiourea synthon directed by π-stacking interactions, crystal structure and Hirshfeld surface analysis, J. Mol. Struct. 1111 (2016) 76-83.

[55] S.S. Parveen, M.A. Al-Alshaikh, C.Y. Panicker, A.A. El-Emam, B. Narayana, V.V. Saliyan, B.K. Sarojini, C. Van Alsenoy, Vibrational and structural observations and molecular docking study on 1-(3-(4-chlorophenyl)-5-[4-(propan-2-yl)phenyl]-4,5-dihydro-1H-pyrazol-1-yl)-ethanone, J. Mol. Struct. 1112 (2016) 136-146.

[56] K.C. Mariamma, H.T. Varghese, C.Y. Panicker, K. John, J. Vinsova, C. Van Alsenoy, Vibrational spectroscopic investigations and computational study of 5-chloro-2-[4-(trifluoromethyl)phenylcarbamoyl]phenyl acetate, Spectrochim. Acta 112 (2013) 161-168.

[57] T. Joseph, H.T. Varghese, C.Y. Panicker, K. Viswanathan, M. Dolezal, T.K. Manojkumar, C. Van Alsenoy, Vibrational spectroscopic investigations and computational study of 5-tert-butyl-N-(4-trifluoromethylphenyl)pyrazine-2-carboxamide, Spectrochim. Acta 113 (2013) 203-214.

[58] G. Varsanyi, Assignments of Vibrational Spectra of Seven Hundred Benzene Derivatives, Wiley, New York, 1974.

[59] R. Renjith, Y.S. Mary, C.Y. Panicker, H.T. Varghese, M. Pakosinska-Parys, C. Van

Alsenoy, A.A. Al-Saadi, Spectroscopic (FT-IR, FT-Raman) investigations and quantum chemical calculations of 1,7,8,9-tetrachloro-10,10-dimethoxy-4-{3-[4-(3-methoxyphenyl)piperazin-1-yl]propyl]-4-azatricyclo[5.2.1.$0^{2,6}$]dec-8-ene-3,5-dione, Spectrochim. Acta 129 (2014) 438-450.

[60] V.S. Madhavan, H.T. Varghese, S. Mathew, J. Vinsova, C.Y. Panicker, FT-IR, FT-Raman and DFT calculations of 4-Chloro-2-(3,4-dichlorophenyl carbamoyl)phenyl acetate, Spectrochim. Acta 72 (2009)547-553.

[61] J.B. Bhagyasree, J. Samuel, H.T. Varghese, C.Y. Panicker, M. Arisoy, O. Tempiz-Arpaci, Synthesis, FT-IR investigations and computatonal stud of 5-[(4-bromophenyl)acetamido]-2-(4-tert-butylphenyl)benzoxazole, Spectrochim. Acta 115 (2013) 79-91.

[62] Y. Ataly, D. Avci, A. Basoglu, Linear and nonlinear optical properties of some donor-acceptor oxadiazoles by ab initio Hartree-Fock calculations, Struct. Chem. 19 (2008) 239-246.

[63] H.O. Kalinowski, S. Berger, S. Braun, Carbon-13 NMR Spectroscopy, John Wiley and Sons, Chichester, 1988.

[64] M. Szafran, A. Komasa, E.B. Adamska, Crystal and molecular structure of 4-carboxypiperidinium chloride (4-piperidinecarboxylic acid hydrochloride), J. Mol. Struct. 827 (2007) 101-107.

[65] S. Nithyanandan, P. Kannan, Photo switchable pendant furyl and thienyl fulgimides containing polypyrroles, Polym. Degrad. Stab. 98 (2013) 2224-2231.

[66] S.H.R. Sebastian, M.A. Al-Alshaikh, A.A. El-Emam, C.Y. Panicker, J. Zitko, M. Dolezal, C. Van Alsenoy, Spectroscopic, quantum chemical studies, Fukui functions, in vitro antiviral activity and molecular docking of 5-chloro-N-(3-nitrophenyl)pyrazine-2-carboxamide, J. Mol. Struct. 1119 (2016) 188-199.

[67] R.G. Parr, R.G. Pearson, Absolute hardness: companion parameter to absolute electronegativity, J. Am. Chem. Soc. 105 (1983) 7512-7561.

[68] I. Fleming, Frontier Orbital and Organic Chemical Reactions, John Wiley and Sons, Berlin, 1976.

[69] J.S. Murray, K. Sen, Molecular Electrostatic Potential, Concepts and Applications, Elsevier, Amsterdam, 1996.

[70] J.M. Seminario, Recent Development and Applications of Modern Density Functional Theory, vol.4, Elsevier, 1996.

[71] N. Okulik, A.H. Jubert, Theoretical analysis of the reactive sites of non-steroidal anti-inflammatory drugs, Internet Electron. J. Mol. Des. 4 (2005) 17-30.

[72] P. Sjoberg, J.S. Murray, T. Brinck, P. Politzer, Average local ionization energies on the molecular surfaces of aromatic systems as guides to chemical reactivity, Canadian J. Chem. 68 (1990) 1440-1443.

[73] P. Politzer, F. Abu-Awwad, J.S. Murray, Comparison of density functional and Haratree-Fock average local ionization energies on molecular surfaces, Int. J. Quantum Chem. 69 (1998) 607-613.

[74] A. Saeed, A. Khurshid, J.P. Jasinski, C.G. Pozzi, A.C. Fantoni, M.F. Erben, Competing intramolecular NHOC hydrogen bonds and extended intermolecular network in 1-(4-chlorobenzoyl)-3-(2-methyl-4-oxopentan-2-yl)thiourea analyzed by experimental and theoretical methods, Chem. Phys. 431-432 (2014) 39-46.

[75] A. Michalak, F. De Proft, P. Geerlings, R. Nalewajski, Fukui functions from the relaxed Kohn-Sham orbitals, J. Phys. Chem. A103 (1999) 762-771.

[76] E.D. Glendening, A.E. Reed, J.E. Carpenter, F.Weinhold, NBO Version 3.1, Gaussian Inc., Pittsburgh, PA, 2003.

[77] M.F. Erben, R. Boese, C.O.D. Vedova, H. Oberhammer, H. Willner, Toward an intimate understanding of the structural properties and conformation preference of oxoesters and thioesters, gas and crystal structure and conformational analysis of dimehtyl monothiocarbonate, $CH_3OC(O)SCH_3$, J. Org. Chem. 71(2) (2006) 616-622.

[78] C. Adant, M. Dupuis, J.L. Bredas, Ab initio study of the nonlinear optical properties of urea : Electron correlation and dispersion effects, Int. J. Quantum. Chem. 56 (1995) 497-507.

[79] M. Li, *Organic chemistry of drug degradation*. 2012: Royal Society of Chemistry.

[80] T. Andersson, A. Broo, E. Evertsson, Prediction of drug candidates sensitivity toward autoxidation: computational estimation of C-H dissociation energies of carbon centered radicals, J. Pharm. Sci. 103 (2014) 1949-1955.

[81] J.S. Wright, H. Shadnia, L.L. Chepelev, Stability of carbon centered radicals, effect of functional groups on the energetic of addition of molecular oxygen, J. Comput. Chem. 30 (2009) 1016-1026.

[82] Y.-R. Luo, *Handbook of bond dissociation energies in organic compounds*. 2002: CRC press.

[83] R.V. Vaz, J.R. Gomes, C.M. Silva, Molecular dynamics simulation of diffusion coefficients and structural properties of ketones in supercritical CO_2 at infinite dilution, J. Supercritic. Fluids 107 (2016) 630-638.

[84] C. Alkan, Y. Tek, D. Kahraman,Preparation and characterization of a series of thiourea derivatives as phase change materials for thermal energy storage, Turkish J. Chem. 35(5) (2011) 769-777.

[85] W.M. Khairul, S.M. Jasman, T. Tagg, K. Kubulat, Naphthoyl-thiourea thin films as potential OLED featuring methyl pyridine moiety, Adv. Mater. Res. 1107 (2015) 672-677.

[86] N. Busschaert, S.J. Bradberry, M. Wenzel, C.J.E. Haynes, J.R. Hiscock, I.L. Kirby, L.E. Karagiannidis, S.J. Moore, N.J. Wells, J. Hermiman, G.J. Langley, P.N. Horton, M.E. Light, I. Marques, P.J. Costa, V. Felix, J.G. Frey, P.A. Gale, Towards predictable transmembrane transport, QSAR analysis of anion binding and transport, Chem. Sci. 4(8) (2013) 3036-3045.

[87] L. Wang, G. Nan, X. Yang, Q. Peng, Q. Li, Z. Shuai, Computational methods for design of organic materials with high charge mobility, Chem. Soc. Rev. 39 (2010) 423-434.

[88] V. Coropceanu, J. Cornil, D.A. da Silva Filho, Y. Olivier, R. Silbey, J.-L. Brédas, Charge transport in organic semiconductors, Chem. Rev. 107 (2007) 926-952.

[89] A. Lagunin, A. Stepanchikova, D. Filimonov, V. Poroikov, PASS: Prediction of activity spectra for bioligically active substances, Bioinformatics 16 (2000) 747-748.

[90] S.B. Singh, W. Liu, X. Li, T. Chen, A. Shafiee, S. Dreikorn, V. Hornak, M. Meinz, J.C. Onishi, Structure activity relationship of cytochrome bc 1 reductase inhibitor broad spectrum antifungal ilicicolin H, Bioorg. Med. Chem. Lett. 23 (2013) 3018-3022.

[91] E. Rodriguez-Fernandez, J.L. Manzano, J.J. Benito, R. Hermosa, E. Monte, J.J. Criado, Thiourea, triazole and thiadiazine compounds and their metal complexes as antifungal agents, J. Inorg. Biochem. 99 (2005) 1558-1572.

[92] I.V. Kulakov, O.A. Nurkenov, S.B. Akhmetova, R.B. Seidakhmetova, Z.M. Zhambekov, Synthesis and antibacterial and antifungal activities of thiourea derivatives of the alkaloid anabasine, Pharm. Chem. J. 45 (2011) 15-18.

[93] O. Trott, A. J. Olson, AutoDock Vina: Improving the speed and accuracy of docking with a new scoring function, efficient optimization and multithreading, J. Comput. Chem. 31 (2010) 455-461.

[94] B. Kramer, M. Rarey, T. Lengauer, Evaluation of the FlexX incremental construction algorithm for protein ligand docking, PROTEINS: Struct. Funct. Genet. 37 (1999) 228-241.

Figure captions

Fig.1 FT-IR spectrum of 1-(3,4-dichlorophenyl)-3-[3-(trifluoromethyl)phenyl]thiourea

Fig.2 FT-Raman spectrum of 1-(3,4-dichlorophenyl)-3-[3-(trifluoromethyl)phenyl]thiourea

Fig.3 Molecular geometries of the five lowest energy conformers of ANF-6 molecule

Fig.4 Optimized geometry of the lowest energy conformer of 1-(3,4-dichlorophenyl)-3-[3-(trifluoromethyl)phenyl]thiourea

Fig.5 HOMO-LUMO plots of 1-(3,4-dichlorophenyl)-3-[3-(trifluoromethyl)phenyl]thiourea

Fig.6 MEP plot of 1-(3,4-dichlorophenyl)-3-[3-(trifluoromethyl)phenyl]thiourea

Fig.7 Representative ALIE surface of ANF-6 molecule

Fig.8 Fukui functions of ANF-6 molecule a)f^+ and b)f^-

Fig.9 BDE of all single acyclic bonds for ANF-6 molecule

Fig.10 RDFs of atoms ofANF-6 molecule with significant interactions with water molecules a) carbon atoms and b) non-carbon atoms

Fig.11 Interactive plot of ligand and cytochrome reductase

Fig.12 Surface view of the docked ligand embedded in the catalytic site of cytochrome reductase

Table 1. Ground state energies of the five lowest energy conformers and their difference, ΔE , in comparison with the lowest energy conformer

Conformer	Ground state energy[a.u.]	ΔE [a.u.]	ΔE [kJ/mol]
ANF-6_33	–2266.550883	0.000084	6.0386
ANF-6_34	–2266.550967	0.000000	0.000000
ANF-6_35	–2266.550946	0.000021	1.5753
ANF-6_46	–2266.550911	0.000056	3.9382
ANF-6_47	–2266.550914	0.000053	3.6757

Table 2

Calculated scaled wave numbers, observed IR, Raman bands and assignments

B3LYP/6-31G(d,p)			IR	Raman	Assignments[a]
υ(cm^{-1})	IRI	RA	υ(cm^{-1})	υ(cm^{-1})	-
3478	61.74	370.40	3420	-	υNH(100)
3434	53.37	1155.38	3226	3222	υNH(99)
3129	1.11	110.83	3137	3130	υCHII(98)
3103	0.45	631.57	-	-	υCHI(99)
3098	4.13	1159.56	-	-	υCHII(99)
3093	0.29	136.41	-	-	υCHI(94)
3090	2.18	19.17	3088	3084	υCHI(99)
3076	2.00	105.56	-	-	υCHII(99)
3075	11.10	228.00	3045	3063	υCHII(94)
1606	41.29	91.43	-	1603	υPhII(59)
1592	0.96	116.53	1592	-	υPhII(63)
1579	47.33	163.52	1572	1582	υPhI(69)
1548	40.75	137.07	-	1550	υPhI(69)
1529	531.62	1331.57	1532	1528	δNH(66)
1481	227.76	198.58	-	1483	δCHII(21), υPhII(53)
1470	300.95	121.67	1470	1471	δNH(47), υCN(23)
1450	128.65	798.67	1455	1451	δCHI(29), υPhI(54)
1411	1.55	129.03	-	1420	υPhII(45), δCHII(24)
1379	46.75	667.85	1385	1381	υPhI(53), δCHI(26)
1327	207.31	261.03	1325	1325	υPhII(63)
1304	158.79	94.44	-	-	δCHII(38), υCN(54)
1300	372.79	54.33	-	-	υCC(33), υCF_3(13), υCN(11)
1285	53.09	121.70	1290	1286	υPhI(46), δCHI(15), δCHII(13)
1277	130.08	257.88	-	1271	υCN(21), υPhI(45)
1248	28.18	469.18	1250	1239	δCHI(66), υPhI(21)
1223	38.11	19.40	-	-	υCN(45), δCHI(18), δCHII(15)
1195	73.94	612.28	1188	1203	δCHI(17), υCN(40)

1170	218.66	602.02	-	-	υCF_3(64)
1159	30.17	2758.17	1163	1162	δCHII(47), υCF_3(10)
1152	158.90	86.81	-	-	υCN(43), υCS(13), δCHII(29)
1140	252.83	98.38	-	1140	υCF_3(73)
1130	11.13	116.29	-	1132	δCHI(60), υPhI(23)
1109	94.76	200.62	1099	1099	δCHI(44), υPhI(41)
1083	39.18	847.80	1078	1078	δCHII(45), υPhII(20)
1056	68.78	263.13	1040	-	υPhII(10), υCF_3(35), δCHII(36)
1005	26.18	27.32	999	1002	δPhI(60), υCCl(16), υPhI(16)
980	2.92	117.71	-	977	δPhII(15), υPhII(65)
966	1.12	51.58	968	-	γCHII(85), τPhII(10)
943	6.26	135.03	945	945	γCHI(22), υCS(11), υPhII(17)
937	2.40	29.11	-	-	γCHI(75)
896	1.74	163.23	905	-	γCHII(87)
884	32.23	253.00	886	885	υCCl(14), υPhI(13), υCN(12), γCHI(11)
869	15.79	112.74	-	867	γCHII(66), τPhII(18)
855	26.52	130.47	858	-	γCHI(64), τPhI(14)
811	22.21	361.13	813	814	γCHI(81)
785	20.49	60.74	788	790	γCHII(66), τPhII(19)
782	2.91	106.90	780	782	δNH(15), δPhII(32)
728	15.41	32.68	728	729	δNH(15), υCS(35)
702	8.47	7.65	708	708	υCS(15), δPhI(26), τPhI(15), υCCl(15)
690	16.84	157.91	693	-	τPhI(29), τPhII(29)
688	13.42	27.82	684	688	τPhI(35), τPhII(25), υCCl(33)
670	15.17	40.44	-	672	δCF_3(37), δNH(16), δPhII(18)
654	5.24	134.88	656	658	δPhI(40), υCCl(40), τPhI(11)
635	12.84	131.53	633	-	δPhII(43), δCF_3(16)
616	16.68	204.47	610	620	γCN(24), τCS(17), τPhII(19, γNH(10)

596	14.91	131.82	-	590	γCS(47), γNH(12)
575	13.91	67.39	577	577	γCN(25), τPhII(31), γCCl(28)
556	0.50	893.59	553	553	δCF_3(53), δPhII(34)
533	11.16	333/17	-	-	γNH(48), τCN(13), γCS(19)
508	15.20	142.60	510	511	δCN(12), δCCl(15), δPhI(21)
505	93.59	379.53	-	-	τCS(22), τNH(37), δCF_3(11), τPhII(13)
493	72.99	45.45	-	-	τPhII(15), δCF_3(40), γCN(28)
471	14.82	86.13	470	468	υCCl(23), δPhII(13), δCS(10), δCCl(10)
443	1.90	78.85	-	446	τPhI(37), γCCl(10), δCCl(13)
442	1.37	67.60	440	440	τPhII(50), δCF_3(23)
430	1.82	161.84	428	428	τPhI(44), γCCl(17)
389	2.60	68.57	-	386	δCF_3(36), δCS(15), δPhI(21)
374	0.84	40.08	-	-	γCCl(11), δCN(11), δPhI(26)
346	2.92	68.81	-	350	δPhII(15), δCF_3(38)
316	1.65	57.35	-	320	τPhII(22), γCCl(13), δCF3(15), δCN(10)
312	0.74	119.64	-	-	τPhII(30), δCF_3(17), γCCl(10)
297	3.23	31.68	-	-	δCF_3(19), δCN(14), δPhI(30)
252	0.09	19.92	-	255	τPhII(32), δPhI(10), δCS(10)
229	0.47	12.98	-	-	δCF_3(12), δCS(12), δCN(10), δCC(10)
211	2.58	139.08	-	210	δCCl(19), δCN(12), τPhII(32)
189	3.47	138.79	-	193	δCCl(58), τPhI(10)
175	1.08	34.35	-	176	δCC(32), δNH(14), δCF_3(10)
171	1.88	94.46	-	168	τPhI(29), γCCl(15), γCN(31)
140	2.45	17.85	-	142	τPhI(28), δNH(14), τPhII(27)
123	0.15	14.62	-	-	γCC(41), δCF_3(17)
94	1.83	96.77	-	93	τPhI(32), τNH(23)
78	3.22	30.71	-	-	τNH(36), γNH(16), δCN(11),

					δCC(10)
42	2.87	143.05	-	-	τCS(24), τCN(22), γNH(31), τPhI(10)
34	0.50	19.19	-	-	τCS(30), τCF_3(16), γNH(33)
26	0.10	68.60	-	-	τCF_3(47), τCN(13), δNH(12)
20	0.78	25.43	-	-	τNH(37), τCN(29), δNH(10)
10	0.06	19.22	-	-	τNH(45), τCF_3(22), τCN(12)

[a]υ-stretching; δ-in-plane deformation; γ-out-of-plane deformation; τ-torsion; PhI-tri-substituted phenyl ring; PhII-1,3-disubstituted phenyl ring; IR_I-IR intensity in KM/Mole; R_A-Raman activity in $Å^4$/AMU; Potential energy distribution (>10%) is given in the assignment column.

Table 3

Optoelectronic properties of urea, thiourea and ANF-6 molecules

Structure	λ_- (eV)	λ_+ (eV)	t (eV)	k_{ET}^- (s^{-1})	k_{ET}^+ (s^{-1})
Urea	0.94	0.27	0.25	3.20×10^{11}	3.67×10^{13}
Thiourea	0.80	0.33	0.15	2.92×10^{11}	2.01×10^{13}
ANF-6	0.40	0.46	0.09	5.64×10^{12}	3.28×10^{12}

Table 4

PASS prediction for the activity spectrum of the title compound. Pa represents probability to be active and Pi represents probability to be inactive

Pa	Pi	Activity
0.912	0.004	Phobic disorders treatment
0.763	0.046	Ubiquinol-cytochrome-c reductase inhibitor
0.706	0.036	Membrane permeability inhibitor
0.658	0.015	Insulysin inhibitor
0.615	0.008	Atherosclerosis treatment
0.615	0.016	HMGCS2 expression enhancer
0.600	0.025	Chloride peroxidase inhibitor
0.559	0.004	CTGF expression inhibitor
0.556	0.002	HDL-cholesterol increasing
0.562	0.019	Platelet derived growth factor receptor kinase inhibitor
0.553	0.018	Analgesic.non-opioid
0.545	0.022	Polarisation stimulant
0.522	0.006	RNA-directed RNA polymerase inhibitor
0.516	0.003	Potassium channel (Ca-activated) activator
0.533	0.031	Analgesic

Table 5

The binding affinity values of different poses of the titlecompound predicted by Autodock Vina.

Mode	Affinity (kcal/mol)	Distance from best mode (Å)	
-	-	RMSD l.b.	RMSD u.b.
1	-6.3	0.000	0.000
2	-6.1	10.478	11.799
3	-6.1	5.579	8.012
4	-6.1	3.966	5.530
5	-5.8	5.484	7.750
6	-5.8	1.300	1.548
7	-5.7	5.023	7.552
8	-5.7	8.124	9.536
9	-5.6	7.918	9.939

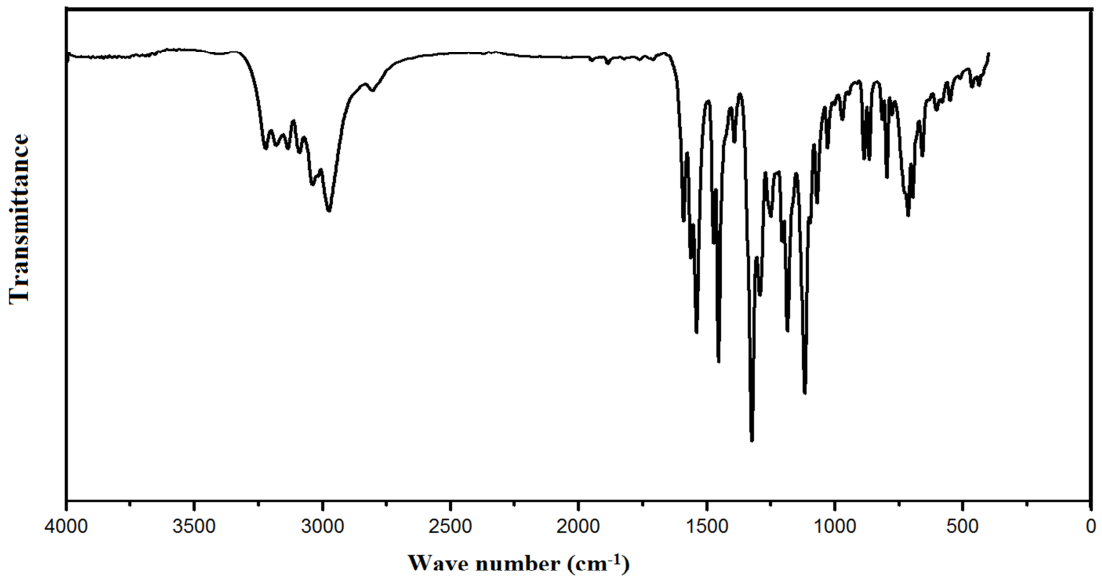

Fig.1 FT-IR spectrum of 1-(3,4-dichlorophenyl)-3-[3-(trifluoromethyl)phenyl]thiourea

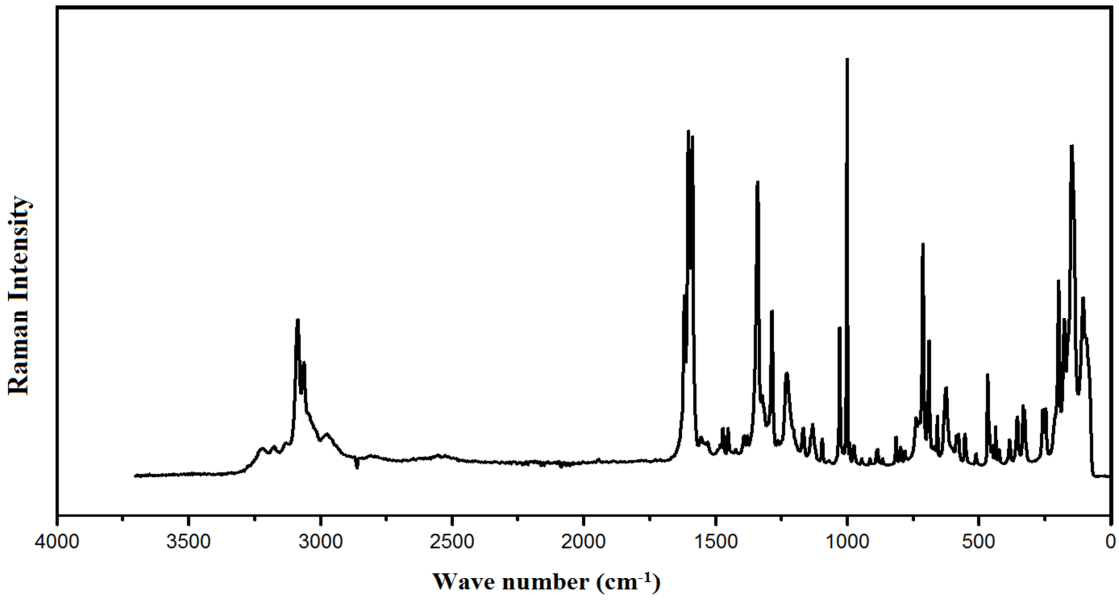

Fig.2 FT-Raman spectrum of 1-(3,4-dichlorophenyl)-3-[3-(trifluoromethyl)phenyl]thiourea

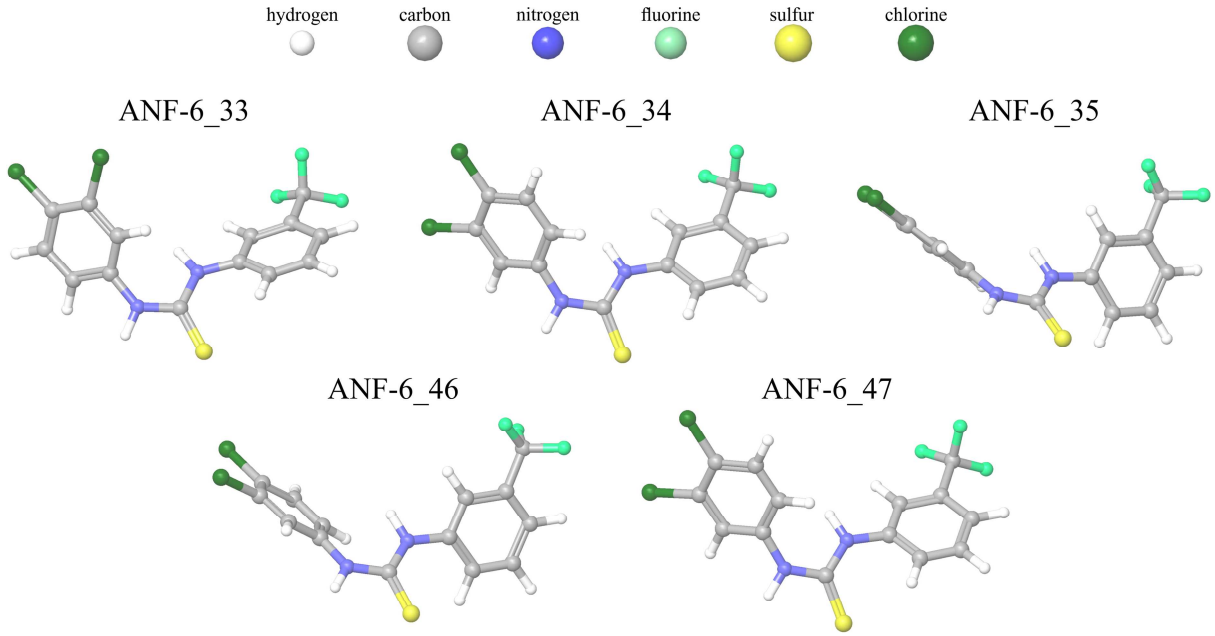

Fig.3 Molecular geometries of the five lowest energy conformers of ANF-6 molecule

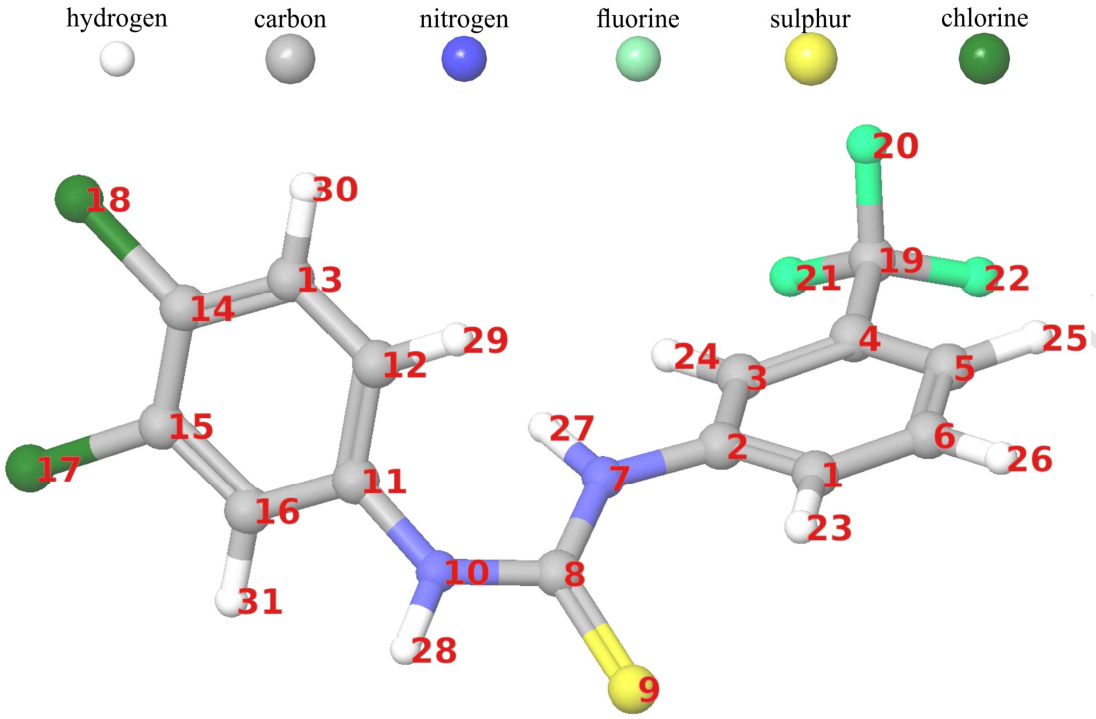

Fig.4 Optimized geometry of the lowest energy conformer of 1-(3,4-dichlorophenyl)-3-[3-(trifluoromethyl)phenyl]thiourea

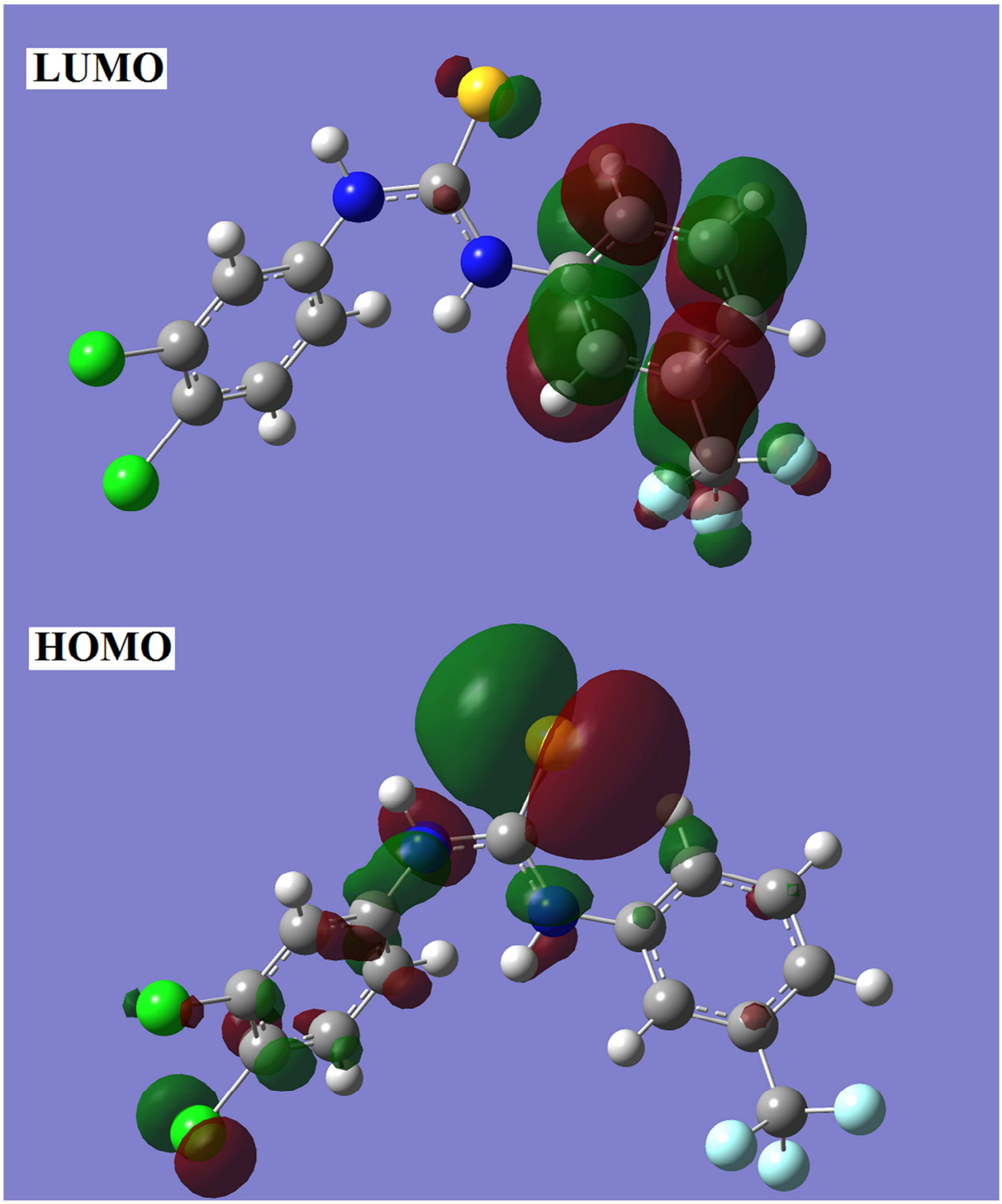

Fig.5 HOMO-LUMO plots of 1-(3,4-dichlorophenyl)-3-[3-(trifluoromethyl)phenyl]thiourea

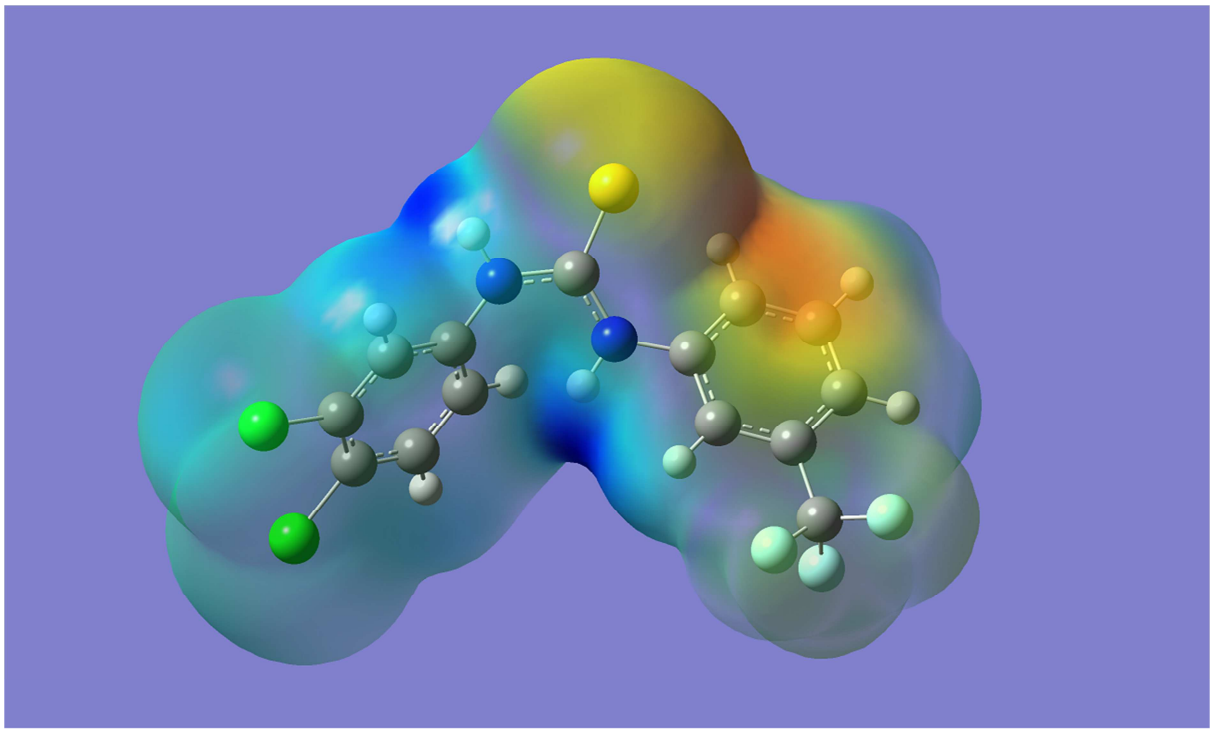

Fig.6 MEP plot of 1-(3,4-dichlorophenyl)-3-[3-(trifluoromethyl) phenyl]thiourea

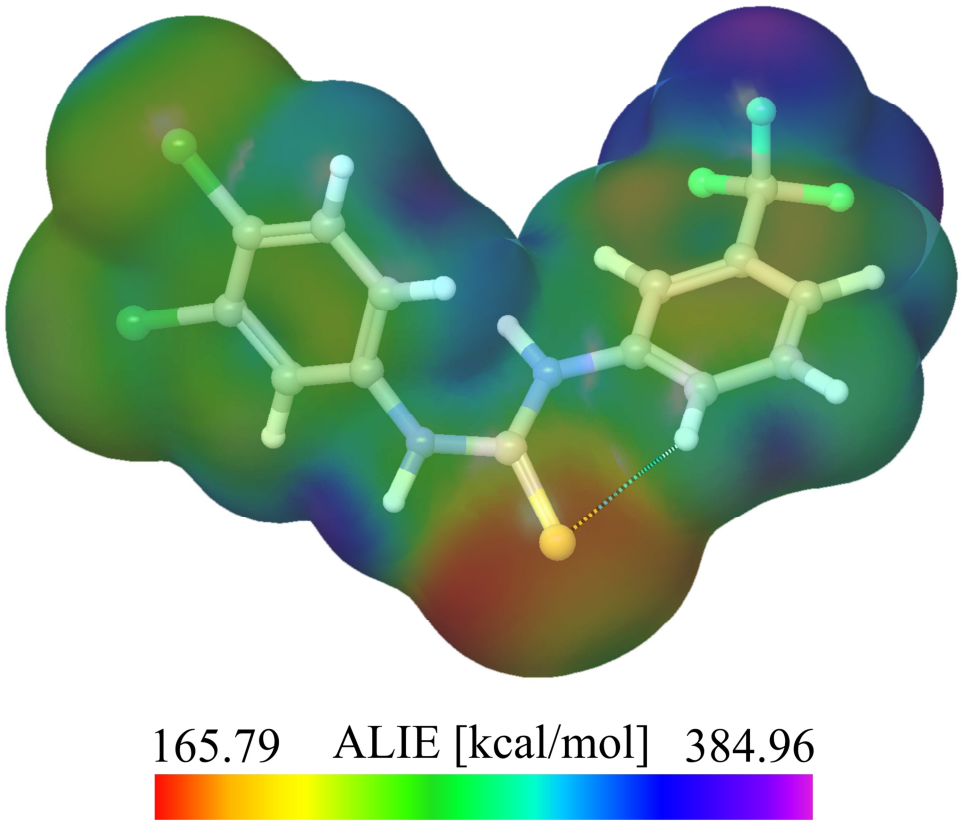

Fig.7 Representative ALIE surface of ANF-6 molecule

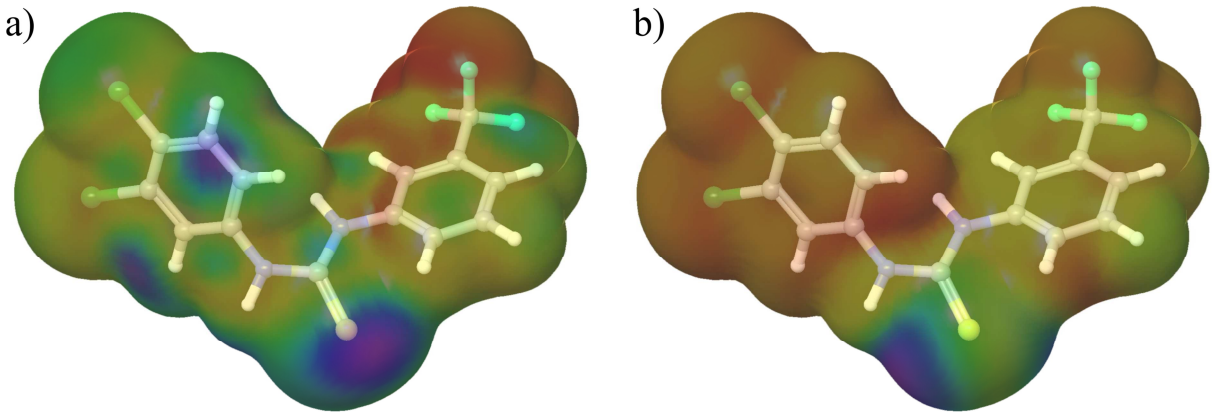

Fig.8 Fukui functions of ANF-6 molecule a)f^+ and b)f^-

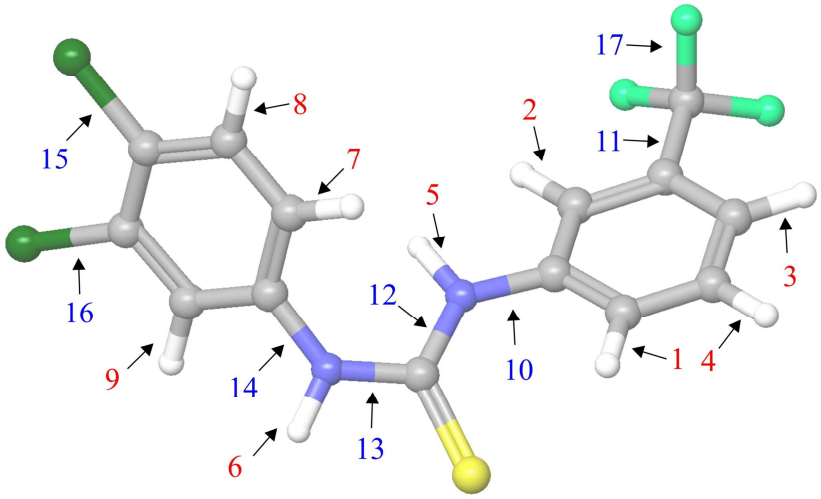

Bond	BDE [kcal/mol]
1	112.01
2	118.90
3	119.53
4	118.12
5	91.56
6	92.22
7	116.66
8	118.84
9	119.60
10	93.17
11	106.94
12	69.06
13	69.55
14	89.47
15	89.25
16	88.48
17	113.81

Fig.9 BDE of all single acyclic bonds for ANF-6 molecule

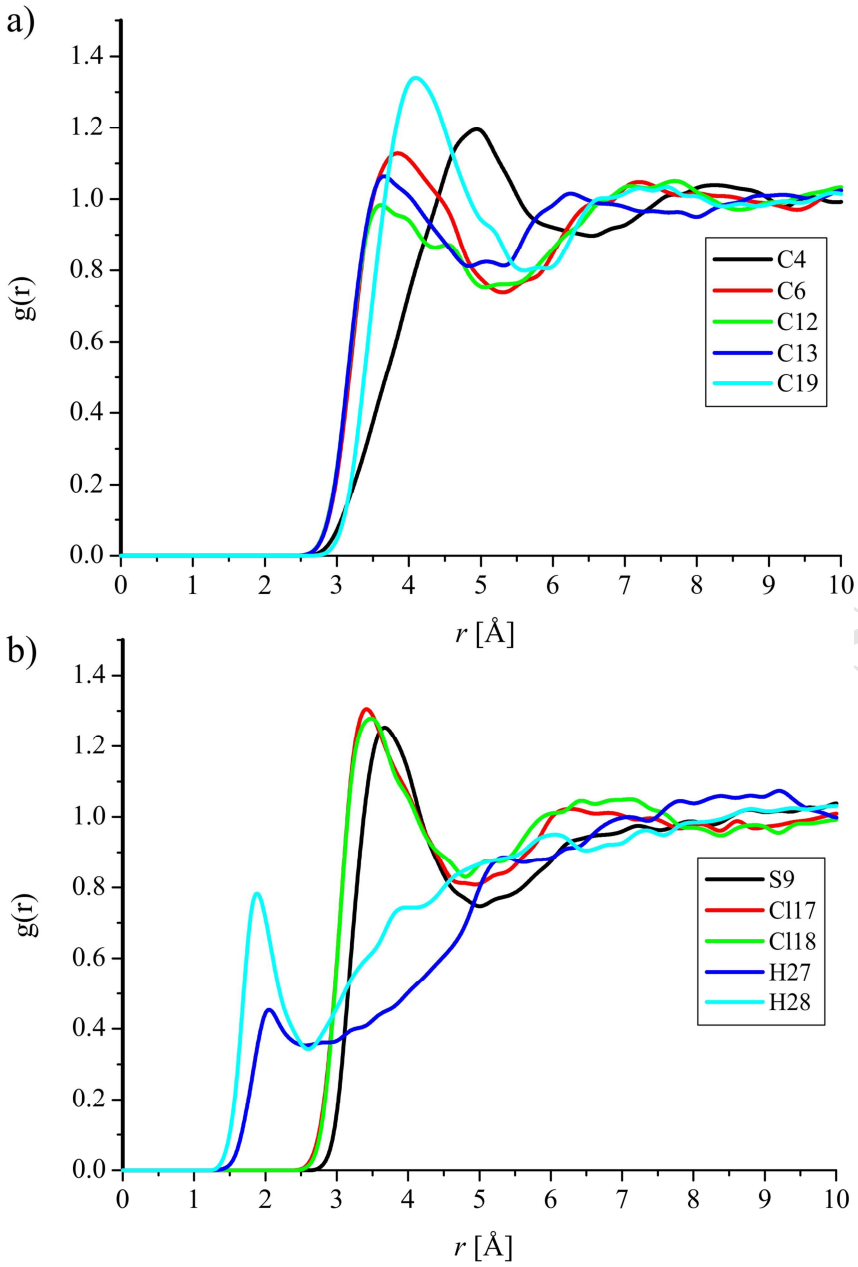

Fig.10 RDFs of atoms ofANF-6 molecule with significant interactions with water molecules a) carbon atoms and b) non-carbon atoms

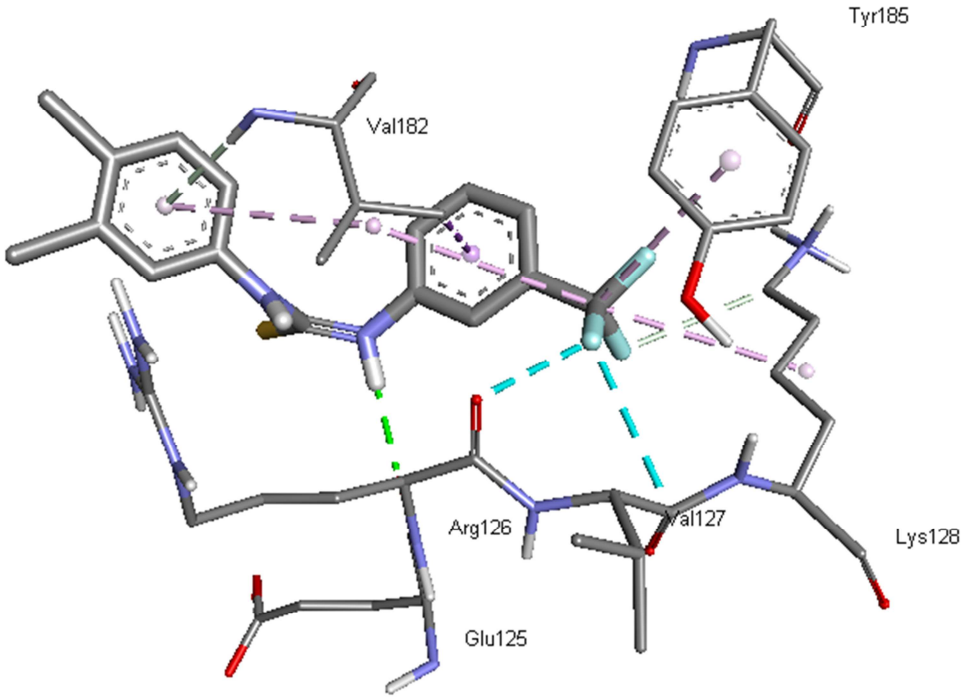

Fig.11 Interactive plot of ligand and cytochrome reductase

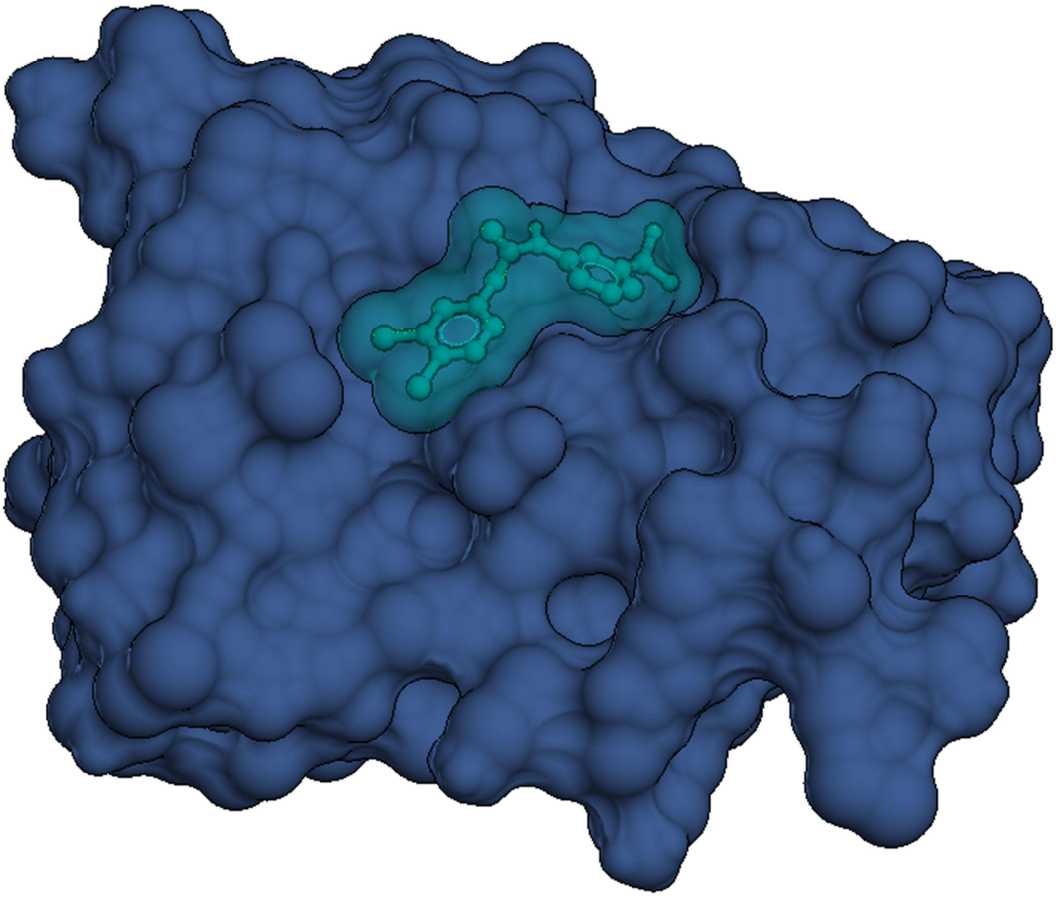

Fig.12 Surface view of the docked ligand embedded in the catalytic site of cytochrome

Highlights

* IR and Raman spectra were measured
* The experimental results were compared with theoretical calculations results.
* ALI, BDE, RDF have been discussed in detail
* PASS analysis predicts cytochrome reductase activity